

1 **Pigments, elemental composition (C, N, P, Si) and**  
2 **stoichiometry of particulate matter, in the naturally iron**  
3 **fertilized region of Kerguelen in the Southern Ocean**

4  
5 **M. Lasbleiz<sup>1</sup>, K. Leblanc<sup>1</sup>, S. Blain<sup>2,3</sup>, J. Ras<sup>4,5</sup>, V. Cornet-Barthaux<sup>1</sup>, S. Hélias**  
6 **Nunige<sup>1</sup>, B. Quéguiner<sup>1</sup>**

7 [1]{Aix-Marseille Université, Université de Toulon, CNRS/INSU, IRD, MIO, UM 110,  
8 13288, Marseille, Cedex 09, France }

9 [2]{Sorbonne Universités, UPMC Univ Paris 06, UMR 7621, Laboratoire d'Océanographie  
10 Microbienne, Observatoire Océanologique, F-66650 Banyuls-sur-mer, France }

11 [3]{CNRS, UMR 7621, Laboratoire d'Océanographie Microbienne, Observatoire  
12 Océanologique, F-66650 Banyuls-sur-mer, France }

13 [4]{Laboratoire d'Océanographie de Villefranche, UMR7093, CNRS, 06230 Villefranche-  
14 sur-Mer, France }

15 [5]{Université Pierre et Marie Curie (Paris-6), Unité Mixte de Recherche 7093, Laboratoire  
16 d'Océanographie de Villefranche-sur-Mer, 06230, Villefranche-sur-Mer, France }

17 Correspondence to: M. Lasbleiz (marine.lasbleiz@univ-amu.fr)

18  
19 **Abstract**

20 The particulate matter distribution and phytoplankton community structure of the iron-  
21 fertilized Kerguelen region were investigated in early austral spring (October-November  
22 2011) during the KEOPS2 cruise. The iron-fertilized region was characterized by a complex  
23 mesoscale circulation resulting in a patchy distribution of particulate matter. Integrated  
24 concentrations over 200 m ranged from 72.2 to 317.7 mg m<sup>-2</sup> for chlorophyll *a*, 314 to  
25 744 mmol m<sup>-2</sup> for biogenic silica (BSi), 1,106 to 2,268 mmol m<sup>-2</sup> for particulate organic  
26 carbon, 215 to 436 mmol m<sup>-2</sup> for particulate organic nitrogen, and 29.3 to 39.0 mmol m<sup>-2</sup> for  
27 particulate organic phosphorus. Three distinct high biomass areas were identified: the coastal  
28 waters of Kerguelen Islands, the easternmost part of the study area in the Polar Front Zone,

1 and the southeastern Kerguelen Plateau. As expected from previous artificial and natural iron-  
2 fertilization experiments, the iron-fertilized areas were characterized by the development of  
3 large diatoms revealed by BSi size–fractionation and HPLC pigment signatures, whereas the  
4 iron-limited reference area was associated to a low biomass dominated by a mixed  
5 (nanoflagellates and diatoms) phytoplankton assemblage. A major difference from most  
6 previous artificial iron fertilization studies was the observation of much higher Si:C, Si:N, and  
7 Si:P ratios (respectively  $0.31 \pm 0.16$  ,  $1.6 \pm 0.7$  and  $20.5 \pm 7.9$ ) in the iron-fertilized areas  
8 compared to the iron-limited reference station (respectively 0.13, 1.1, 5.8). A second  
9 difference is the patchy response of the elemental composition of phytoplankton communities  
10 to large scale natural iron fertilization. Comparison to the previous KEOPS1 cruise also  
11 allowed to address the seasonal dynamics of phytoplankton bloom over the southeastern  
12 plateau. From POC, PON, and BSi evolutions, we showed that the elemental composition of  
13 the particulate matter also varies at the seasonal scale. This temporal evolution followed  
14 changes of the phytoplankton community structure as well as major changes in the nutrient  
15 stocks progressively leading to silicic acid exhaustion at the end of the productive season.

16 Our observations suggest that the specific response of phytoplankton communities under  
17 natural iron fertilization is much more diverse than what has been regularly observed in  
18 artificial iron fertilization experiments and that the elemental composition of the bulk  
19 particulate matter reflects phytoplankton taxonomic structure rather than being a direct  
20 consequence of iron availability.

21

## 22 **1 Introduction**

23 Considered as the largest High Nutrient Low Chlorophyll (HNLC) region in the world, the  
24 Southern Ocean is characterized by low phytoplankton productivity despite nutrient-rich  
25 waters (Martin et al., 1991; Sarmiento et al., 2004). The “Iron Hypothesis” is now largely  
26 acknowledged to explain this paradox. Martin et al. (1990) estimated that new production  
27 could be enhanced about 30-fold under iron-replete conditions and could thus stimulate the  
28 export of carbon (C) to the deep ocean by fixing atmospheric CO<sub>2</sub>. This hypothesis motivated  
29 several artificial iron (Fe) enrichment experiments in different HNLC areas all over the world  
30 (Boyd et al., 1999; Takeda, 1998; de Baar et al., 2005; Boyd, 2007; Smetacek et al., 2012).  
31 All these studies confirmed that addition of Fe stimulated phytoplankton growth but only one

1 postulated an enhanced C sequestration on the sea floor (Smetacek et al., 2012). This could  
2 result from experimental artifacts, and especially from the shorter duration of experiments  
3 compared to that of vertical export processes.

4 To overcome those experimental constraints, the concept of “natural fertilization laboratory”  
5 was coined by Blain et al. (2007). The objective was to investigate the response of ecosystem  
6 functioning and biogeochemical cycles in a naturally iron-fertilized system by comparison  
7 with a nearby typical HNLC environment. In the early 2000s, five projects addressed this  
8 concept in different regions of the Southern Ocean: the Kerguelen Ocean and Plateau  
9 compared Study (KEOPS1) (Blain et al., 2007), the CROZet natural iron bloom and EXport  
10 experiment (CROZEX) (Pollard et al., 2009), the Blue Water Zone (BWZ) program (Zhou et  
11 al., 2010; 2013), the Discovery 2010 cruises (Tarling et al., 2012), and the Dynamic Light on  
12 Fe limitation (DynaLiFe) project (Arrigo and Alderkamp, 2012). Each of these studies  
13 focused on recurrent seasonal blooming regions characterized by large bathymetric  
14 discontinuities (such as ridges, islands and/or submarine plateaus) and strong hydrodynamic  
15 forcings (especially geostrophic fronts), which together interact and generate natural iron  
16 inputs to surface waters. The natural iron enrichment experiments consistently verified an  
17 enhanced efficiency of C export within the naturally Fe-fertilized systems which was  
18 approximately 3-times higher than in the surrounding Fe-limited areas (Morris and Charette,  
19 2013). However, some gaps still persist regarding the understanding of the factors controlling  
20 the dynamics of phytoplankton blooms in naturally Fe-fertilized systems of the Southern  
21 Ocean.

22 Previous studies in the literature have documented the influence of iron on both the structure  
23 and the elemental ratios of phytoplankton communities. The phytoplankton community  
24 structure is known to directly impact the fate of carbon through sinking rates depending on  
25 various factors such as cell size, ballast minerals, transparent exopolymers (TEP), or  
26 (re)packaging in zooplankton fecal pellets (Margalef, 1965; Falkowski et al., 2003; Legendre  
27 and Le Fèvre, 1989; Armstrong et al., 2009). Artificial and natural iron-fertilization  
28 experiments evidenced the preferential development of large diatoms (> 20 µm) under iron-  
29 replete conditions (Hutchins and Bruland, 1998; Takeda, 1998; Hare et al., 2005; Armand et  
30 al., 2008; Timmermans et al., 2008). In a recent review paper, Quéguiner (2013) proposed a  
31 conceptual general scheme for phytoplankton development in naturally Fe-fertilized systems  
32 where phytoplankton are separated into two groups occupying different niches in the water

1 column according to their adaptation to limiting proximal factors (iron, silicic acid, and light)  
2 and their resistance to grazing by micro- and mesozooplankton. Diatoms are responsible for  
3 more than 40 % of the global oceanic primary production (Nelson et al., 1995). Large diatoms  
4 favor the export and sequestration of carbon (Nelson et al., 1995; Buesseler, 1998). Diatom  
5 growth can be controlled by silicic acid ( $\text{H}_4\text{SiO}_4$ ) availability, an essential nutrient for the  
6 formation of diatom frustules. Together Fe and  $\text{H}_4\text{SiO}_4$  could be co-limiting (Dugdale et al.,  
7 1995) and could directly alter the stoichiometry of biogenic matter by influencing the uptake  
8 rates of major elements. Both artificial and natural iron-fertilization experiments reported  
9 higher Si:C, Si:N and Si:P ratios under Fe-stress compared to Fe-replete conditions (Hutchins  
10 and Bruland, 1998; Franck et al., 2000; Moore et al., 2007). Thus, Fe limitation seemed to  
11 promote the development of more heavily silicified diatoms by strongly enhancing the Si  
12 compared to C and N uptake rates (de Baar et al., 1997; Firme et al., 2003). However, some  
13 exceptions were soon documented. For example, Hutchins et al. (1998) observed that Fe  
14 could sometimes limit phytoplankton growth without changing the Si:C and Si:N ratios. The  
15 control of phytoplankton elemental ratios in response to iron availability therefore remains  
16 poorly understood, which clearly calls for new observations.

17 During the first KEOPS cruise (KEOPS1), conducted in January-February 2005, the impact of  
18 iron on  $\text{H}_4\text{SiO}_4$  and nitrate ( $\text{NO}_3^-$ ) utilization by diatoms was investigated in the southeastern  
19 part of the naturally iron-fertilized Kerguelen Plateau (Mosseri et al., 2008; Timmermans et  
20 al., 2008). In this area, an annual bloom of diatoms depleting dissolved inorganic carbon  
21 (DIC) in surface waters (Jouandet et al., 2008) is sustained by continuous iron inputs at the  
22 surface thanks to the enhanced vertical inputs of iron-rich deep waters from the plateau (Blain  
23 et al., 2007; Park et al., 2008a). Unexpectedly, Mosseri et al. (2008) reported moderate  
24 differences in elemental ratios (Si:C:N) of the particulate matter between Fe-fertilized waters  
25 and HNLC waters. This observation was attributed to the combined effects of the presence of  
26 an already decaying diatom bloom over the plateau, and the presence of heavily silicified  
27 diatoms in HNLC waters.  $\text{H}_4\text{SiO}_4$ :DIC and  $\text{H}_4\text{SiO}_4$ : $\text{NO}_3^-$  elemental uptake ratios of the  
28 natural diatom community of the plateau were close to 0.13 and 1 respectively, as expected  
29 for diatoms growing in nutrient-replete conditions (Hutchins and Bruland, 1998; Takeda,  
30 1998). However, the high  $\text{NO}_3^-$  concentrations in surface waters compared to  $\text{H}_4\text{SiO}_4$   
31 depletion at the end of the bloom suggested a strong decoupling between the seasonal  
32 consumption of these two nutrients. According to Mosseri et al. (2008), this could be due to

1 differential remineralisation between Si and N and by the capacity of diatoms to grow  
2 preferentially on ammonium, thereby preventing the complete utilization of the winter  $\text{NO}_3^-$   
3 stock. In the context of the “silicic acid leakage hypothesis” of Matsumoto et al. (2002), this  
4 unexpected decoupling between  $\text{H}_4\text{SiO}_4$  and  $\text{NO}_3^-$  consumptions, if extended over the entire  
5 Permanently Open Ocean Zone (POOZ) of the Southern Ocean, could have large implications  
6 at global scale in the control of low latitude productivity and phytoplankton assemblages  
7 (Sarmiento et al., 2004). Moreover, understanding this decoupling is of critical importance to  
8 assess the efficiency of Fe fertilization in terms of DIC uptake at regional and global scales.

9 In order to follow up on KEOPS1 observations, the second KEOPS cruise (KEOPS2) was  
10 conducted in the naturally iron-fertilized region of Kerguelen Plateau (KP) during austral  
11 spring (October-November) 2011. Focused east of the Kerguelen Islands (KI), the study  
12 investigated the biogeochemical cycles and phytoplankton community structures in contrasted  
13 environments differently impacted by iron availability and mesoscale activity. In this paper,  
14 we examine the particulate matter distribution in relation to the phytoplankton community  
15 structure in these contrasted environments. By combining KEOPS1 data corresponding to the  
16 late stage of the bloom, the temporal evolution of phytoplankton community over the KP will  
17 be documented during the entire blooming period. The aim is to assess the seasonal degree of  
18 coupling between C, N, P, and Si cycles to better understand the seasonal dynamics of  
19 phytoplankton blooms in naturally Fe-fertilized region. The use of lithogenic silica as a proxy  
20 for lithogenic matter is discussed to track potential sources of Fe in the KP region.

## 21 **2 Method**

### 22 **2.1 Sampling strategy**

23 The KEOPS2 cruise was conducted in austral spring from October 10<sup>th</sup> to November 20<sup>th</sup>  
24 2011 aboard the R/V Marion Dufresne (TAAF/IPEV). This research project was focused east  
25 of the KP which is characterized by the passage of the Polar Front (PF), as illustrated in  
26 Fig. 1. The KP region is surrounded by the Antarctic Circumpolar Current (ACC) whose main  
27 branch circulates to the north of the plateau (Park et al., 2008b). A southern branch of the  
28 ACC circulates to the south of Kerguelen Islands to further join a branch of the Fawn Trough  
29 Current (FTC). The FTC has a main northeast direction, but a minor branch splits away  
30 northwestward to rejoin the eastern side of the KP (Park et al., 2008b). These particular

1 hydrographic features generate contrasted environments which are differently impacted by  
2 iron availability and mesoscale activity. Among these contrasted environments, KEOPS2  
3 focused on the northeastern Kerguelen bloom (E stations), the eastern bloom (F-L and F-S  
4 stations) in the Polar Front Zone (PFZ), and the southeastern KP bloom (A3 station). The  
5 latter was visited twice (A3-1 in October and A3-2 in November) at a reference station that  
6 had been already studied during the KEOPS1 cruise. For comparison, the station R2 was  
7 considered as representative of the HNLC off-plateau area. A temporal evolution study of the  
8 northeastern Kerguelen bloom was led on the complex recirculation system located in a  
9 stationary meander of the PF. This site (referred as stations E including E-1, E-2, E-3, E-4E  
10 and E-5) was visited five times in the course of the cruise. Across this complex system, two  
11 transects were sampled to get a detailed description of the biogeochemical parameters of the  
12 eastern Kerguelen area. The first transect, oriented south to north (TNS), was sampled from  
13 21 to 23 October; the second transect, oriented west to east (TEW), was sampled from 31  
14 October to 02 November.

15 Seawater samples were collected using a Seabird *SBE 911-plus* CTD unit mounted on a 24  
16 12-L bottles rosette. A total of 30 different stations were sampled for analysis of particulate  
17 (biogenic and lithogenic) silica, particulate organic matter (carbon, nitrogen and phosphorus)  
18 and biomarker pigments. Sampling was performed at 6 to 24 depths over the water column  
19 and covered a wide range of bottom depths from 84 m to 2,786 m above and off-plateau  
20 respectively.

## 21 **2.2 Biogenic and lithogenic silica stocks**

22 For particulate silica analyses, size fractionation was performed by filtering 2-L seawater onto  
23 stacked 0.8 and 20  $\mu\text{m}$  Nucleopore® polycarbonate filters simultaneously. Samples were  
24 folded in 4 and stored in Eppendorf vials, dried overnight at 60°C before being closed and  
25 stored at room temperature. Biogenic silica (BSi) and lithogenic silica (LSi) were measured  
26 following the triple extraction procedure described by Ragueneau et al. (2005). Dried filters  
27 were digested two times at 95°C for 45 mn with an analysis of both Si and Al concentrations  
28 at each step. In order to correct BSi for LSi contamination, particulate aluminum was  
29 measured in parallel by the Lumogallion fluorescence method of Hydes and Liss (1976)  
30 adapted by Howard et al. (1986). After the double alkaline digestion, a third extraction in  
31 2.9 mol L<sup>-1</sup> hydrofluoric acid was performed on dried filters during 48h. Blank values were

1  $1.0 \pm 0.2 \text{ nmol L}^{-1}$  for BSi,  $16 \pm 7 \text{ nmol L}^{-1}$  for LSi and  $24 \pm 9 \text{ nmol L}^{-1}$  for particulate Al.  
2 This implied detection limits, defined by the sum of the average blank value plus three times  
3 the standard deviation of the blanks, of  $1.6 \text{ nmol L}^{-1}$ ,  $37 \text{ nmol L}^{-1}$  and  $51 \text{ nmol L}^{-1}$  for BSi ,  
4 LSi and particulate Al respectively. For some samples, Al concentrations analyzed after the  
5 second NaOH extraction were inferior to the detection limit. These samples were also  
6 characterized by the lowest LSi concentrations. The correction of the lithogenic interference is  
7 only valid considering that Al content of diatom frustules is negligible as compared to that of  
8 LSi (Schlüter and Rickert, 1998). According to Ragueneau et al. (2005), in the case of low  
9 LSi concentrations, as in open ocean waters, the interference of diatom Al may overestimate  
10 LSi concentrations. For these reasons, we decided not to apply the Al correction for samples  
11 with Al concentrations below the quantification limit, defined by the sum of the average blank  
12 value plus ten times the standard deviation of the blanks ( $114 \text{ nmol L}^{-1}$ ). This concerns  
13 especially off-plateau stations far from the influence of Kerguelen Islands.

### 14 **2.3 Particulate organic carbon (POC), nitrogen (PON) and phosphorus (POP)**

15 For POC and PON measurements, 1-L seawater samples were collected. For POP  
16 measurements 0.5-L seawater samples were collected. Samples were filtered onboard on 25-  
17 mm Whatman GF/F filters (precombusted at  $450^\circ\text{C}$ ) and stored in precombusted glass vial.  
18 Filters were dried several days at  $60^\circ\text{C}$ , then sealed with an aluminium cap and stored at room  
19 temperature. In order to remove inorganic carbon, POC/PON filters were acidified with  
20 fuming HCl. Finally, POC and PON concentrations were determined using the combustion  
21 method of Strickland and Parsons (1972) on an EA 2400 CHN Analyzer. POP filters were  
22 digested following the wet oxidation method described by Pujo-Pay and Raimbault (1994).  
23 Extracts were clarified through  $0.2\text{-}\mu\text{m}$  Nucleopore® polycarbonate filters before being  
24 analyzed on a 3-SEAL autoanalyzer. Blanks were  $1.27 \pm 0.26 \mu\text{mol L}^{-1}$  for POC,  
25  $0.06 \pm 0.02 \mu\text{mol L}^{-1}$  for PON and  $0.011 \pm 0.005 \mu\text{mol L}^{-1}$  for POP. The detection limits,  
26 defined as above, were  $2.05$  and  $0.12 \mu\text{mol L}^{-1}$  for POC and PON and  $0.026 \mu\text{mol L}^{-1}$  for POP.  
27 Most samples collected below 100 m showed POC concentrations inferior to the  
28 quantification limit ( $3.87 \mu\text{mol L}^{-1}$ ). To compare integrated concentrations of particulate  
29 matter over the same depth (200 m), we decided to estimate these low POC concentrations as  
30 the minimum detectable concentration ( $2.05 \mu\text{mol L}^{-1}$ ). This approximation seems reasonable  
31 considering that PON and POP standing stocks were mostly concentrated in the upper 100 m.

## 1 **2.4 Pigment measurements**

2 For pigment analyses, seawater samples were filtered through 25-mm Whatman GF/F filters.  
3 The filtered volumes varied from 1-L to 2.2-L according to the charge in particles. Filters  
4 were then placed in cryotubes and stored in liquid nitrogen. In the laboratory, pigments were  
5 extracted and analyzed following the procedure of Van Heukelem and Thomas (2001)  
6 modified by Ras et al. (2008). Filters were extracted in 3-mL methanol (100 %) for 2h at  
7 -20°C. The extracts were then vacuum-filtered onto Whatman GF/F filters. Within 24h of  
8 extraction, extracts were analyzed by High Performance Liquid Chromatography (HPLC)  
9 with a complete Agilent Technologies 1200 series system. Separation of pigments was  
10 performed by means of a reversed phase C8 Zorbax Eclipse XDB column (3×150 mm;  
11 3.5 µm particle size). Concentrations were calculated from the peak area obtained by diode  
12 array detection at 450 nm for carotenoids, chlorophylls *c* and *b*, 667 nm for chlorophyll *a* and  
13 derived pigments and 770 nm for bacteriochlorophyll *a*. An internal standard correction  
14 (Vitamine E acetate, Sigma) and external calibration standards (provided by DHI Water and  
15 Environment in Denmark) were applied for calculations of pigment concentrations. This  
16 method enabled detection of 25 pigments with low detection limits (varying from 0.1 ng L<sup>-1</sup>  
17 for chlorophyll *b* to 0.4 ng L<sup>-1</sup> for chlorophyll *a* and alloxanthin, considering a filtered volume  
18 of 1-L of seawater). Following the methods of Claustre (1994) and Vidussi et al. (2001)  
19 modified by Uitz et al. (2006), seven diagnostic pigments were used as biomarkers of specific  
20 phytoplankton taxa to assess the contribution of three pigment-based size classes (micro-,  
21 nano-, and picophytoplankton) to the total phytoplankton biomass. The seven pigments are  
22 fucoxanthin (Fuco), peridinin (Peri), alloxanthin (Allo), 19'-butanoyloxyfucoxanthin (19'BF),  
23 19'-hexanoyloxyfucoxanthin (19'HF), zeaxanthin (Zea), and total chlorophyll *b* (TChl *b*).  
24 Microphytoplankton (> 20 µm) is associated to Fuco and Peri pigments. Nanophytoplankton  
25 (2-20 µm) is associated to Allo, 19'BF and 19'HF pigments. Picophytoplankton (< 2 µm) is  
26 associated to Zea and TChl *b* pigments.



## 1 **3 Results**

### 2 **3.1 Phytoplankton pigments: biomass and community composition**

#### 3 **3.1.1 Spatial variability over the study area**

4 The study area was characterized by an heterogeneous distribution of vertically integrated  
5 chlorophyll *a* concentrations (Chl *a*, in Fig. 2a). It is important to keep in mind that this  
6 overview of the study area was also influenced by the rapid temporal evolution of the  
7 phytoplankton blooms. The TNS transect and station A3-1 were sampled at the start of the  
8 bloom, ten days before sampling the TEW transect including stations F-L and F-S. Satellite  
9 images (d'Ovidio et al., 2012) revealed that during the TEW transect, the bloom was rapidly  
10 developing with a large spatial heterogeneity.

11 The lowest integrated Chl *a* concentrations were found at the off-plateau stations R2  
12 (39.0 mg m<sup>-2</sup>) and TNS-1 (52.1 mg m<sup>-2</sup>). Maximum concentrations were observed at TEW-7  
13 (223.0 mg m<sup>-2</sup>) and F-L (353.8 mg m<sup>-2</sup>), evidencing a very high phytoplankton biomass in the  
14 PFZ. The Polar Front clearly isolated these very high Chl *a* waters from comparatively lower  
15 Chl *a* southern waters (ranging from 100.0 to 187.7 mg m<sup>-2</sup>).

16 In the same way, the study area was characterized by an heterogeneous distribution of  
17 phytoplankton communities as revealed by pigment biomarkers (Figs. 2b, 2c and 2d). The  
18 phytoplankton community was mainly dominated by microphytoplankton (representing on  
19 average 83 % of total Chl *a* biomass) all over the study area. The microphytoplankton  
20 contribution was however clearly lower at stations R2 and TNS-1 (47 and 39 % of total Chl *a*  
21 biomass respectively) due to a higher proportion of nanophytoplankton (39 and 41 % of total  
22 Chl *a* biomass respectively). Stations TNS-1 and TNS-2 also departed from this general trend  
23 by exhibiting a higher picophytoplankton contribution (~20 % of total Chl *a* biomass) as  
24 compared to the other stations (<10 % of total Chl *a* biomass).

25 Chl *a* : Fuco ratios ( $2.3 \pm 0.4$ ; data not shown) were within the typical range of values (1.1 to  
26 2.3) for diatoms (Wright and Jeffrey, 1987; Tester et al., 1995; Ediger et al., 2001) except for  
27 the off-plateau stations R2 and TNS-1, where higher ratios ( $4.3 \pm 0.8$ ) were found.  
28 Fucoxanthin is the dominant biomarker for diatoms but is also found in some  
29 prymnesiophytes (e.g. *Phaeocystis* sp.), chrysophytes (e.g. silicoflagellates such as *Dictyocha*  
30 sp.) and dinoflagellates. The very low concentrations in 19'BF, 19'HF and peridinin at all

1 stations (ranging from 0.8 to 9.7, 1.9 to 12.8 and 0.4 to 3.2 mg m<sup>-2</sup> respectively) compared to  
2 fucoxanthin (20.9 to 160.2 mg m<sup>-2</sup>) clearly evidence the dominance of diatoms over the other  
3 classes of phytoplankton all over the study area, except at R2 and TNS-1. At these stations,  
4 Chl *a* : 19'BF (12.0 ± 1.4), and Chl *a* : 19'HF (4.4 ± 0.1) ratios were the lowest of the study  
5 area, reflecting the higher contribution of nanoflagellates to the phytoplankton community  
6 (data not shown).

### 7 3.1.2 Vertical distributions along transects TNS and TEW

8 The vertical distribution of Chl *a* along transects TNS and TEW are presented in Fig. 3 and  
9 Fig. 4 respectively. For both transects, the higher concentrations (> 0.5 mg m<sup>-3</sup>) were  
10 restricted to the upper 150 m and were clearly dominated by microphytoplankton  
11 communities.

12 At the beginning of the bloom, Chl *a* concentrations ranged from 0.5 to 1.5 mg m<sup>-3</sup> in the  
13 upper 100 m from TNS-3 to TNS-6 and in the upper 180 m from TNS-7 to TNS-10 following  
14 the mixed layer depth (Fig. 3). North of the PF, Chl *a* concentrations were lower reaching 0.6  
15 mg m<sup>-3</sup> in the upper 60 m at TNS-2 and 0.3 mg m<sup>-3</sup> over 200 m depth at TNS-1. TNS-1 was  
16 very different from the rest of the transect with higher contributions of nanophytoplankton  
17 over 150 m (20 to 50 % contribution to total biomass depending on depth; Fig. 5). Ten days  
18 later, higher phytoplankton biomasses (up to 5.0 mg m<sup>-3</sup>) were observed in the PF area  
19 between TEW-7 and TEW-8 (Fig. 4). Vertical profiles clearly evidenced the PF influence  
20 which isolated very high Chl *a* waters to the north from comparatively lower Chl *a* waters to  
21 the south. The coastal station TEW-1 was also characterized by very high Chl *a*  
22 concentrations within the first 40 m (up to 4.7 mg m<sup>-3</sup>). As shown by satellite images  
23 (d'Ovidio et al., 2012), TEW-1 already supported a large phytoplankton bloom before the  
24 beginning of the cruise, likely due to precocious favorable growth conditions in the coastal  
25 zone. The latter was separated from the off-plateau waters by the southern branch of the PF  
26 circulating along the shelf-break between TEW-3 and TEW-4. The PF signature along the  
27 shelf break was defined by lower Chl *a* concentrations (< 1.0 mg m<sup>-3</sup>). Maximum  
28 concentrations in fucoxanthin (2.0 to 2.5 mg m<sup>-3</sup>) were similarly found for both the eastern  
29 area north of the PF and at station TEW-1, indicating the dominance by diatoms (Fig. 6). The  
30 core of the TEW transect (TEW-4 to TEW-6) was characterized by Chl *a* concentrations  
31 ranging from 1.0 to 1.5 mg m<sup>-3</sup> at the surface and a significant increase of the

1 nanophytoplankton contribution to the total biomass (20 to 30 %; Fig. 6). An increased  
2 grazing activity was evidenced at TEW-7 and TEW-8 by relatively higher concentrations in  
3 phaeopigments (Phaeo); the ratio of Phaeo to Chl *a* was indeed higher (0.3) at these sites as  
4 compared to all other stations ( $< 0.1$ ; data not shown).

### 5 3.1.3 Temporal evolution at contrasted productive stations

6 No clear temporal evolution of the phytoplankton biomass could be evidenced in the complex  
7 system of recirculation located in the stationary meander of the PF, as demonstrated by the  
8 integrated Chl *a* concentrations (ranging between 98.2 and 129.0 mg m<sup>-2</sup>) from the first (E-1)  
9 to the last (E-5) visit in Fig. 7.

10 Stations E-4W and A3 were visited two times (Fig. 7). The largest phytoplankton  
11 development was observed at the KP reference station A3, where Chl *a* concentrations have  
12 increased 3.5-fold over one month (from 106.2 mg m<sup>-2</sup> in October, A3-1 visit, to 371.7 mg m<sup>-2</sup>  
13 in November, A3-2 visit). This evolution was accompanied by an increase of the  
14 Phaeo : Chl *a* ratio (from  $< 0.1$  to 0.3), reflecting a higher grazing activity at the second visit  
15 (data not shown).

16 Station E-4W was characterized by a moderate evolution compared to A3, likely due to the  
17 shorter period of time between the two sampling periods (6 days compared to 27 days). Chl *a*  
18 concentrations increased about 2-fold from 131.2 to 249.8 mg m<sup>-2</sup> between the two visits.

19 For A3 station and E stations, the temporal evolution of chlorophyll biomass was mainly due  
20 to the development of a microphytoplankton community largely dominated by diatoms. At  
21 these stations, integrated nano- and picophytoplankton biomasses, determined using  
22 diagnostic pigments, were very low and nearly constant all over the course of the cruise  
23 (respectively  $14.4 \pm 3.7$  and  $4.6 \pm 1.7$  mg m<sup>-2</sup>; Fig. 7).

## 24 3.2 Biogenic silica and particulate organic matter

### 25 3.2.1 Spatial variability over the study area

26 The study area was characterized by an heterogeneous distribution of biogenic silica (BSi)  
27 and particulate organic carbon (POC), nitrogen (PON) and phosphorus (POP) (Fig. 8). The  
28 lowest vertically integrated concentrations of BSi, POC, and PON were measured at the off-  
29 shore stations R2 and TNS-1 with integrated values over 200 m of 88.6 mmol Si m<sup>-2</sup>, 610.5

1 mmol C m<sup>-2</sup>, and 78.1 mmol N m<sup>-2</sup> respectively. The lowest concentrations of POP were  
2 evidenced at the station TEW-3 (8.9 mmol P m<sup>-2</sup> over 200 m). The highest concentrations  
3 were observed between TEW-7 and TEW-8 (250.4 to 377.6 mmol Si m<sup>-2</sup> for BSi, 1,200 to  
4 1,875 mmol C m<sup>-2</sup> for POC, 214.7 to 354.4 mmol N m<sup>-2</sup> for PON, 29.5 to 39.0 mmol P m<sup>-2</sup> for  
5 POP), confirming the very high phytoplankton biomass of the PF area. North of the KP, the  
6 distribution of BSi, POC, PON and POP was influenced by the passage of the PF which  
7 isolated northern waters characterized by low particulate matter concentrations from southern  
8 waters characterized by high particulate matter concentrations. This feature is especially  
9 highlighted for BSi concentrations (Table 1).

### 10 3.2.2 Vertical distribution along transects TNS and TEW

11 At the beginning of the bloom, along the TNS transect, POC, PON and POP concentrations  
12 were low at all stations (< 12 μmol C L<sup>-1</sup>, < 1.5 μmol N L<sup>-1</sup> and < 0.16 μmol P L<sup>-1</sup>  
13 respectively; Fig. 9). For BSi concentrations, two contrasted areas were observed on either  
14 side of the PF, with southern waters richer (1.29 to 3.14 μmol Si L<sup>-1</sup>) than northern waters  
15 (0.08 to 1.05 μmol Si L<sup>-1</sup>).

16 Along the TEW transect (Fig. 10), ten days later, the vertical distributions of BSi and  
17 particulate organic matter clearly followed the same pattern as Chl *a*. The highest BSi, POC,  
18 PON and POP concentrations were observed at both the coastal station TEW-1 at the surface  
19 (2.77 to 5.87 μmol Si L<sup>-1</sup>, 5.50 to 16.3 μmol C L<sup>-1</sup>, 1.00 to 2.82 μmol N L<sup>-1</sup>, and 0.15 to  
20 0.22 μmol P L<sup>-1</sup> respectively) and in the PF area between TEW-7 and TEW-8 down to 50 m  
21 depth (2.85 to 5.42 μmol Si L<sup>-1</sup>, 10.1 to 31.9 μmol C L<sup>-1</sup>, 2.42 to 5.89 μmol N L<sup>-1</sup>, 0.23 to  
22 0.81 μmol P L<sup>-1</sup> respectively). The core of the transect (TEW-3 to TEW-6) was characterized  
23 by lower particulate matter concentrations (0.51 to 2.91 μmol Si L<sup>-1</sup>, 3.93 to 11.4 μmol C L<sup>-1</sup>,  
24 0.42 to 2.21 μmol N L<sup>-1</sup> and 0.01 to 0.19 μmol P L<sup>-1</sup>). As noticed for Chl *a* in this area, higher  
25 BSi concentrations (2.32 to 2.91 μmol Si L<sup>-1</sup>) were observed at TEW-4 down to 100 m depth.  
26 Standing out of Chl *a* and particulate organic matter distributions, a well-defined deep BSi  
27 maximum (2.00 ± 0.10 μmol Si L<sup>-1</sup>) was found at 300 m at TEW-5.

28 For both transects, the vertical distribution of BSi strongly paralleled that of fucoxanthin  
29 (Fig. 3), confirming the dominance of diatoms in the phytoplankton communities of the  
30 Kerguelen region. Size-fractionation of BSi can bring information on the sizes of the diatoms  
31 even though the presence of debris can alter this information. Nano-sized fraction of BSi (0.8

1 to 20  $\mu\text{m}$ ) can then correspond to the presence of small diatom species or fragments of  
2 diatoms. Micro-sized fraction of BSi ( $> 20 \mu\text{m}$ ) indicates the presence of large siliceous  
3 phytoplankton which could represent both large diatoms cells and large colonies of diatoms.  
4 In the Kerguelen region, size fractionation of BSi (Fig. 11) revealed the major role played by  
5 large ( $> 20 \mu\text{m}$ ) siliceous phytoplankton which accounted for  $> 60 \%$  of total BSi at all  
6 productive stations over different depths according to the location: down to 200 m at TEW-4,  
7 A3-2, and E (E-1 to E-5) stations (typical vertical profile represented by station TEW-4 in  
8 Fig. 11a), down to 100 m at E-4W and in the PF area (represented by F-L vertical profile in  
9 Fig. 11b), and down to 40 m at TEW-1 (data not shown). The relative contribution of the two  
10 size classes was mainly driven by the evolution of the large size fraction over these different  
11 depths, as the small size fraction concentrations remained fairly constant around  
12  $190 \text{ mmol Si m}^{-2}$ . As a consequence, the nano-sized diatoms (0.8 to  $20 \mu\text{m}$ ) were dominant at  
13 the low productive stations (R2, TNS-1, TNS-2, TEW-2, TEW-3, TEW-5 and TEW-6; typical  
14 vertical profile illustrated by station R2 in Fig. 11c) and everywhere below 200 m except at  
15 station TEW-5 (Fig. 11d). The latter station showed an increasing contribution of the micro-  
16 sized fraction ( $> 20 \mu\text{m}$ ) to total siliceous biomass with depth (ranging from 23 % at the  
17 surface and 60 % between 300 and 400 m). This unusual feature coincided with the deep BSi  
18 maximum mentioned above.

### 19 3.2.3 Temporal evolution at contrasted productive stations

20 Slight increases in BSi (Fig. 12) and particulate organic matter (data not shown)  
21 concentrations were observed in the recirculation system (stations E). From the first (E-1) to  
22 the third visit (E-3), integrated concentrations over 200 m were relatively constant (average:  
23  $308.2 \pm 23.6 \text{ mmol Si m}^{-2}$  for BSi,  $1,065 \pm 51 \text{ mmol C m}^{-2}$  for POC,  $195.6 \pm 11.6 \text{ mmol N m}^{-2}$   
24 for PON and  $13.5 \pm 1.6 \text{ mmol P m}^{-2}$  for POP). Values then increased at the two last visits  
25 (E-4E and E-5), reaching  $410.7 \pm 23.1 \text{ mmol Si m}^{-2}$ ,  $1,651 \pm 26 \text{ mmol C m}^{-2}$ ,  
26  $231.5 \pm 31.0 \text{ mmol N m}^{-2}$  and  $28.5 \pm 5.9 \text{ mmol P m}^{-2}$ . In addition, vertical profiles revealed  
27 that BSi and particulate organic matter were concentrated in a shallow layer (from the surface  
28 down to 100 m depth) during these two last visits (data not shown).

29 As mentioned for Chl *a*, the largest phytoplankton development was observed at A3 with  
30 increasing concentrations of BSi (from 163.5 to  $713.3 \text{ mmol Si m}^{-2}$ ), POC (from 1,259 to  
31  $2,267 \text{ mmol C m}^{-2}$ ), PON (from 137.9 to  $435.9 \text{ mmol N m}^{-2}$ ), and POP (from 9.7 to

1 29.3 mmol P m<sup>-2</sup>) between A3-1 and A3-2 visits (Fig. 12, data not shown for POC, PON and  
2 POP concentrations). On the first visit of E-4W, the situation was already characterized by  
3 high BSi, POC, PON, and POP concentrations over 100 m depth (up to 3.83, 20.0, 3.60,  
4 0.27 μmol L<sup>-1</sup> respectively). The temporal evolution between the two visits was still  
5 considerable with integrated concentrations varying from 379.5 to 744.2 mmol m<sup>-2</sup> for BSi,  
6 1,162 to 1,598 mmol m<sup>-2</sup> for POC, from 288.2 to 354.1 mmol m<sup>-2</sup> for PON, and from 21.5 to  
7 32.6 mmol m<sup>-2</sup> for POP.

8 The temporal evolution of particulate matter in the meander of the PF and at stations A3 and  
9 E-4W evidenced a significant growth of the siliceous phytoplankton community since the  
10 beginning of the cruise. As a general trend, the large size fraction (> 20 μm) was overall  
11 contributing to around 60 % of integrated BSi stocks in the surface productive layer, with the  
12 exception of stations R2 and E-3 where the small size fraction (0.8 to 20 μm) was slightly  
13 dominant (respectively accounting for 59.4 % and 52.5 % of above mentioned integrated BSi  
14 stocks). However, it is particularly important to notice that the BSi stocks located between  
15 200 and 400 m, which may reflect the communities sinking out of the surface layer, were  
16 always dominated by the nano-sized particles (ranging from 61.4 to 86.1 % of BSi stocks  
17 integrated from 200 to 400 m depths).

### 18 **3.3 Elemental ratios of particulate matter**

19 The elemental ratios in the upper 200 m are presented as six clusters of stations (Fig. 13),  
20 grouped in function of biomass, elemental ratios and phytoplankton community structure  
21 reported for each station. The objective of this clustering is to provide an overview of the  
22 distribution of elemental ratios over the study area to highlight some spatial and temporal  
23 patterns. Each cluster of stations includes systems with different environmental dynamics.  
24 Mann-Whitney tests were then performed on these six clusters for each elemental ratio (Si:C,  
25 Si:N, Si:P, C:N, C:P and N:P) to determine the clusters that were significantly different from  
26 each other at the 95% confidence level (Fig. 13). The six clusters of stations corresponded to:  
27 (1) the lowest biomass stations including the off-plateau stations R2 and TNS-1, and A3-1 at  
28 the start of the bloom, (2) the moderate productive stations north of the PF (TNS-2, TEW-2,  
29 TEW-3), (3) the high biomass stations in the PFZ (TEW-7, TEW-8, F-L, F-S), (4) the high  
30 biomass stations south of the PF (A3-2, E-4W, E-4W2), (5) the moderate biomass stations

1 south of the PF (TNS-3 to TNS-10 , E-1 to E-5, TEW-4 to TEW-6), (6) the coastal station  
2 TEW-1.

3 The lowest Si:C, Si:N and Si:P ratios were observed at the lowest biomass stations (cluster  
4 (1)) of the study area in the upper 200 m (respectively  $0.11 \pm 0.07$ ,  $0.67 \pm 0.43$  and  $9.6 \pm 6.4$ ).  
5 Except for cluster (1), Si:C, Si:N and Si:P ratios were always higher than the typical values  
6 for nutrient-replete diatoms (Brzezinski, 1985). The highest average values were observed at  
7 the coastal station TEW-1 in the upper 70 m (cluster (6)) reaching  $0.70 \pm 0.25$  for Si:C,  
8  $2.59 \pm 0.40$  for Si:N and  $34.4 \pm 6.6$  for Si:P. The other stations located north of the PF or in  
9 the PFZ (clusters (2) and (3)) were characterized by lower average Si:C, Si:N and Si:P molar  
10 ratios (respectively  $0.28 \pm 0.01$ ,  $1.32 \pm 0.13$ ,  $16.0 \pm 2.6$ ) than the stations south of the PF  
11 (respectively  $0.35 \pm 0.01$ ,  $1.75 \pm 0.05$ ,  $24.9 \pm 4.3$ ). This observation agreed with statistical  
12 tests: the clusters of the stations north of the PF were statistically different from the other  
13 clusters south of the PF (Fig. 13).

14 Except for the lowest biomass stations (cluster (1)), C:N and C:P ratios were relatively  
15 constant (reaching average values of  $5.1 \pm 1.4$  and  $73.0 \pm 35.4$  respectively) and lower than  
16 the Redfield et al. (1963) ratios. N:P ratios were close to the Redfield's ratio all over the study  
17 area (average:  $14.4 \pm 6.3$ ) except for the stations located in the PFZ (cluster (3)). These  
18 stations were characterized by lower C:P ( $48.1.7 \pm 18.0$ ) and N:P ( $10.5 \pm 3.3$ ) ratios than the  
19 rest of the study area. The Mann-Whitney test did not evidence any significant difference  
20 between the median of the six clusters for C:P and N:P ratios. For C:N ratios, only the low  
21 biomass stations were significantly different from the other stations at the 95 % confidence  
22 level.

23 Over the course of the cruise, the development of diatoms was evidenced between the first  
24 (A3-1) and the second visits (A3-2) at A3 with Si:C and Si:N ratios increasing respectively  
25 from  $0.14 \pm 0.06$  to  $0.32 \pm 0.06$  and  $0.87 \pm 0.25$  to  $1.66 \pm 0.24$  (data not shown). Significant  
26 increases in Si:C and Si:N were also observed at E-4W from the first ( $0.29 \pm 0.12$  for Si:C  
27 and  $1.25 \pm 0.62$  for Si:N) to the second visit ( $0.39 \pm 0.07$  for Si:C and  $2.06 \pm 0.15$  for Si:N).  
28 Moderate increases were shown for Si:P ratio both at A3 (from  $17.3 \pm 2.9$  to  $19.6 \pm 6.7$ ) and  
29 E-4W (from  $18.3 \pm 4.4$  to  $19.4 \pm 6.3$ ). At E-4W, a slight decrease was evidenced from the first  
30 to the second visit for C:N (from  $5.5 \pm 0.5$  to  $5.0 \pm 0.5$ ), C:P (from  $76.3 \pm 12.3$  to  $71.7 \pm 25.7$ )  
31 and N:P (from  $17.1 \pm 6.0$  to  $12.9 \pm 1.9$ ). At A3, higher decrease was observed from the first to

1 the second visit for C:N (from  $8.8 \pm 3.5$  to  $5.3 \pm 0.2$ ), C:P (from  $148.9 \pm 47.2$  to  $65.9 \pm 32.8$ )  
2 and N:P (from  $20.9 \pm 3.1$  to  $11.4 \pm 5.2$ ).

### 3 **3.4 Lithogenic silica**

4 Lithogenic silica is a good proxy to track the transport of lithogenic material (and indirectly  
5 Fe) from terrestrial erosion, aeolian dust deposition or sediment resuspension to the water  
6 column (Quéguiner et al., 1997). Over the entire study area, LSi concentrations did not exceed  
7  $0.11 \mu\text{mol L}^{-1}$  throughout most of the water column, except at stations subjected to continental  
8 influence (Fig. 14). The highest LSi values were observed at the coastal station TEW-1  
9 (average:  $1.31 \pm 0.14 \mu\text{mol L}^{-1}$ ) and at station A3 near the bottom ( $1.34 \pm 0.07 \mu\text{mol L}^{-1}$ ). In  
10 addition, compared to surrounding waters, station A3 was characterized by relatively higher  
11 concentrations down to 300 m (values  $> 0.15 \mu\text{mol L}^{-1}$ ). This feature was also observed at the  
12 second visit A3-2 (Fig. 15). The lowest LSi concentrations were found at TNS-1 with values  
13  $< 0.01 \mu\text{mol L}^{-1}$  over the first 400 m (Fig. 14). As expected, concentrations were low at  
14 station R2 (Fig. 15), located far from any continental influence ( $< 0.04 \mu\text{mol L}^{-1}$  in the upper  
15 100 m), although a maximum was reported at 500 m ( $0.12 \mu\text{mol L}^{-1}$ ). Inside the meander of  
16 the PF (stations E), LSi concentrations were lower than  $0.10 \mu\text{mol L}^{-1}$  but local maxima ( $0.12$   
17  $\text{to } 0.13 \mu\text{mol L}^{-1}$ ) between 600 and 700 m were noticed at the first (E-1), the fourth (E-4E)  
18 and the last visit (E-5) (and likely E-2, although data are missing to confirm it). High LSi  
19 concentrations were also observed at E-4W at 75 m and 400 m ( $0.23$  and  $0.12 \mu\text{mol L}^{-1}$   
20 respectively) only during the second visit. Along the transect TEW, LSi concentrations were  
21 higher in the PFZ reaching values higher than  $0.11 \mu\text{mol L}^{-1}$  over the water column at TEW-8.  
22 As a general trend, LSi was mainly composed of small particles (from 0.8 to 20  $\mu\text{m}$ ) over the  
23 water column, representing in average 59.5 % of total LSi. However, local maximums  
24 observed at A3-2 (50 m), F-L (300 m), E-4W2 (75 and 400 m) and E-5 (600 m) were  
25 associated to large particles ( $> 20 \mu\text{m}$ ), accounting for 65.2 to 86.5 % of the total LSi.

## 26 **4 Discussion**

### 27 **4.1 The Kerguelen Plateau region: a mosaic of biogeochemical environments**

28 The biogeochemical characteristics of the water masses northeast of the Kerguelen Islands  
29 have already been documented by Blain et al. (2001) in early spring (October 1995). They



1 highlighted the complex mesoscale structure of water masses which generated contrasting  
2 biogeochemical environments above the KP. The particular mesoscale circulation is directly  
3 impacted by the topography of the KP and the presence of the PF pathway isolating warm  
4 northern subantarctic surface waters from cold southern Antarctic Surface Water (AASW)  
5 (Park and Gamberoni, 1997). Similar circulation patterns (Park et al., this volume; Zhou et al.,  
6 this volume) were observed during the KEOPS2 cruise. This is probably partly for that reason  
7 that a mosaic of biogeochemical conditions was also encountered.

8 Coastal waters (corresponding to stations TEW-1 and TEW-2) were characterized by a large  
9 diatom bloom and high LSi concentrations, evidencing strong lithogenic material inputs  
10 (including iron) from the plateau.

11 A strong shelf front isolated these warmer coastal waters ( $> 2.4^{\circ}\text{C}$ ) from the cold ( $2.3^{\circ}\text{C}$ ) PF  
12 water tongue containing low Chl *a* and BSi concentrations. Blain et al. (2001) associated this  
13 water tongue (corresponding to station TEW-3 in our study) to an intrusion of AASW where  
14 phytoplankton growth was limited by an unfavorable light-mixing regime. Indeed, TEW-3  
15 showed the deepest mixed layer depth (95 m) of the west-east transect, but unfortunately  
16 photosynthetic parameters were not determined precluding any conclusion about the light  
17 limitation hypothesis. Grazing pressure could also be another limiting factor for  
18 phytoplankton growth. However, zooplankton biomass was too low at TEW-3 (Carlotti et al.,  
19 this volume) to explain the low Chl *a* and BSi concentrations.

20 By contrast, a productive, high-biomass system was found in the eastern area in the PF  
21 between TEW-7 and TEW-8. This area was characterized by a shallow mixed layer (down to  
22 50 m), likely providing favorable light conditions for diatom growth. Despite being far from  
23 the plateau, these stations showed sufficient iron concentrations ( $\sim 0.2 \text{ nmol L}^{-1}$  over 50 m;  
24 Qu  rou   et al., this volume) to support phytoplankton growth. Significant iron could be  
25 supplied by the transport of Fe-rich deep waters from the KP to the northwestern Kerguelen  
26 Abyssal Plain east of the KP (Zhou et al., this volume), but also from the coastal area by  
27 lateral advection driven by the subantarctic surface water eastward flow north of the PF  
28 (Bucciarelli et al., 2001). Potential sources of iron will be discussed in paragraph 4.4.

29 The largest diatom development was observed over the southeast KP at the reference station  
30 A3 (during the second visit) with the highest Chl *a* and BSi concentrations reported during the  
31 cruise. This station also evidenced high LSi concentrations near the bottom suggesting

1 lithogenic material inputs from the plateau sediments. Indeed, one major conclusion of  
2 KEOPS1 was that the long-lasting diatom bloom above the plateau was maintained by the  
3 continuous supply to the surface mixed layer of iron and nutrients. The latter originated from  
4 below due to an enhanced tidally-induced vertical mixing associated to a weak mean residual  
5 circulation resulting in a long retention time for nutrients and trace elements (Blain et al.,  
6 2007; Park et al., 2008a). On a longer time-scale, it was assumed that iron supply to A3  
7 originated from horizontal advection from the extensive shoal around the Heard/Mc Donald  
8 Islands (Park et al., 2008a). East of the KP, this northward circulation along the topography  
9 could also lead to a partial export of the plateau bloom. This feature was supported by the  
10 observation of similar biogeochemical properties at station A3 and at the eastern flank  
11 (corresponding to station E-4W for the two visits) of the KP. The E-4W station evidenced the  
12 same range of values as A3 in terms of BSi, POC, PON, and POP concentrations and quite  
13 similar diatom community compositions mainly dominated by *Chaetoceros Hyalochaete*,  
14 *Thalassiosira*-like (pending SEM determination) and *Pseudo-nitzschia* spp. (Lasbleiz et al., in  
15 prep.). Furthermore, the assemblages in sediments at these two sites were similarly composed  
16 of *Eucampia antarctica*, *Dactyliosolen antarctica*, *Fragilariopsis kerguelensis*, *Chaetoceros*  
17 resting spores, *Rhizosolenia* spp. as well as an uncommon species, *Thalassiosira decipiens*,  
18 not observed anywhere else over the study area (Wilks, 2013). The northward export of part  
19 of the southeast KP bloom also serves as a good explanation to the higher particulate matter  
20 concentrations observed at TEW-4 compared to the other stations of the TEW transect at the  
21 beginning of the cruise.

22 As compared to the easternmost part of the study area in the PF, the stations south of the PF  
23 exhibited moderate biomasses. Inside the meander of the PF, two stages in the development of  
24 the siliceous phytoplankton community were observed in the course of the cruise. At the  
25 beginning, particulate matter concentrations were moderate and slightly decreasing from the  
26 first (E-1) to the third visit (E-3). The microplanktonic size fraction ( $> 20 \mu\text{m}$ ) contribution to  
27 siliceous biomass was also decreasing while the nanoplanktonic size fraction contribution  
28 increased from 34.5 % at the first visit (E-1) to 47.5 % of the siliceous biomass at the third  
29 visit (E-3) (Fig. 12). By contrast, the two last visits (E-4E and E-5) showed an increase in  
30 phytoplankton biomass dominated by large diatoms and concentrated over a shallower depth.  
31 Closset et al. (this volume) also reported these two contrasted periods through the  $\int\text{D}:\text{P}$  ratio  
32 defined as the ratio of Si dissolution rates (D) to Si production rates (P) integrated over the

1 euphotic zone. From E-1 to E-3, increasing  $\int$ D:P ratio evidenced an increased BSi loss due to  
2 enhanced BSi dissolution in surface waters, while decreasing  $\int$ D:P ratio between E-4E and E-  
3 5 resulted from enhanced BSi production rates and revealed bloom conditions. Together,  
4 these results would suggest that the start of the bloom period (E-4E and E-5) was preceded  
5 by a non-lasting phytoplankton development before the first sampling (E-1). This short bloom  
6 event could have been aborted by adverse hydrodynamic conditions before the beginning of  
7 the cruise. This was consistent with the increase in the proportion of empty diatoms frustules  
8 from E-1 to E-3 (from 5.1 % to 25.7 %; Lasbleiz et al., in prep.) and the increase of  
9 phytodetrital and fecal aggregates observed at depth by Laurenceau et al. (this volume). The  
10 important role of mesoscale structures and turbulence in the control of primary production  
11 and light availability have already been reported by previous studies (e.g. Lancelot et al.,  
12 2000; Lévy et al., 2001; Read et al., 2007). We hypothesize that the instability of the mixed  
13 layer depth before the beginning of the cruise could have generated deepening events  
14 providing unfavourable light conditions for phytoplankton growth. Our hypothesis is  
15 supported by the  $\sigma_\theta$  profiles which indicate the existence of a secondary pycnocline around  
16 130 m at E-1 and a continuous gradient with no clear mixed layer from the surface down to  
17 200 m depth E-3 (data not shown). Furthermore, the slight increase in zooplankton abundance  
18 from E-1 to E-3 (Carlotti et al., this volume) suggests that phytoplankton growth was not  
19 mainly impacted by grazing pressure. Another feature of the area south of the PF was the  
20 presence of a minimum of biomass in the central core of the complex recirculation meander  
21 (corresponding to station TEW-5). This central core stands out from the rest of the study area  
22 by the presence of a deep silica maximum (between 300 and 400 m; Fig. 10a) mainly  
23 associated to microplanktonic size particles ( $> 20 \mu\text{m}$ ). There could be several explanations  
24 for this peculiar feature. (1) Given the low Si biomass at the surface, the presence of large and  
25 non-living diatoms at depth could reflect the sedimentation of an early bloom that could have  
26 been quickly driven to an end due to adverse hydrodynamic conditions, as discussed above. A  
27 vertical net haul down to 100 m depth at TEW-5 revealed the dominance of the heavily  
28 silicified diatoms *Fragilariopsis kerguelensis* as well as *Corethron pennatum* (Armand L.,  
29 pers. comm., 2013). However no sediment sample was collected at this station to evidence  
30 their eventual influence on vertical export. (2) Mesoscale activity could also have favored the  
31 transfer and the accumulation of biogenic silica at depth in the central meander area which is  
32 characterized as a region of general downwelling (Zhou et al., this volume). (3) Finally, the

1 northward circulation from the KP could have advected large and non-living diatoms already  
2 sedimenting at depth coming from productive southern waters.

## 3 **4.2 Impact of natural iron enrichment on Chl *a* and phytoplankton** 4 **communities**

### 5 4.2.1 The off-plateau HNLC stations

6 During the KEOPS2 cruise, the off-plateau station R2 showed the lowest chlorophyll biomass  
7 ( $39.0 \text{ mg m}^{-2}$ ; Fig. 2a) despite high macronutrient concentrations of the surrounding waters  
8 (Blain et al., this volume). In this HNLC area, one limiting factor was likely iron availability  
9 as suggested by the low iron concentrations in surface waters ( $\sim 0.1 \text{ nmol L}^{-1}$ ; Qu  rou   et al.,  
10 this volume) and the Fe-Cu incubation experiments (Bowie et al., this volume; Sarthou et al.,  
11 this volume). Light could also have been (co-)limiting as the mixed layer extended down to  
12  $\sim 120 \text{ m}$  almost exactly coinciding with the 0.01 % surface light level. Chl *a* concentrations  
13 were in the same order of magnitude as that measured in typical HNLC waters of the  
14 Southern Ocean (Bathmann et al., 1997; Gall et al., 2001; Froneman et al., 2004) and more  
15 specifically, of the Kerguelen region (Cailliau et al., 1997; Uitz et al., 2009). Integrated  
16 chlorophyll biomass was however higher than the lowest values corresponding to the poorest  
17 areas of the Southern Ocean (range:  $10 \text{ to } 20 \text{ mg m}^{-2}$ ) suggesting the slight phytoplankton  
18 development that may have occurred shortly before the site visit. In contrast to the other  
19 stations of the study area, the off-plateau station R2 showed a lower microphytoplankton  
20 contribution (47 % of total Chl *a* biomass; Fig. 2b) due to a higher proportion of  
21 nanophytoplankton (39 % of total Chl *a* biomass; Fig. 2c). This result was expected from  
22 previous artificial and natural iron-fertilization experiments (Gall et al., 2001; Hoffmann et  
23 al., 2006; Moore et al., 2007; Lance et al., 2007). Increased contributions of nano-sized  
24 communities (small diatoms or flagellates) were reported under iron limited conditions  
25 (Sunda and Huntsman, 1997; Timmermans et al., 2001; Armand et al., 2008; Uitz et al.,  
26 2009). Cell counts confirmed the dominance of nanoflagellates at station R2 in terms of C  
27 biomass (Lasbleiz et al., in prep.). Several species of dinoflagellates and the silicoflagellate  
28 *Dyctiocha speculum* were also important contributors to C biomass compared to diatoms. At  
29 station R2, the Chl *a* : Fuco ratio (3.7) and Chl *a* : 19'BF ratio (11.0) were respectively higher  
30 and lower than those measured for diatoms (Wright and Jeffrey, 1987; Ediger et al., 2001).

1 Such Chl *a* : Fuco and Chl *a* : 19'BF ratios have been reported for dinoflagellates in previous  
2 studies (Johnsen and Sakshaug, 1993; Ediger et al., 2001).

3 Like the station R2, the off-plateau station TNS-1 was distinguished from the study area by its  
4 low chlorophyll biomass (52.1 mg m<sup>-2</sup>; Fig. 2a) and higher proportion of nano- (41 %) and  
5 pico- (20 %) phytoplankton (Fig. 2c et 2d). Even if there are no available data to confirm it, a  
6 limitation by iron seems almost likely given the tenuity of the surface mixed layer (from 20 to  
7 35 m), the high abundance of macronutrients (Blain et al., this volume) and the low grazing  
8 pressure (Carlotti et al., this volume). At station R2 and TNS-1, the picophytoplankton  
9 contribution to chlorophyll biomass was higher (up to 20 %) than in the rest of the study area  
10 but relatively low by comparison to previous studies in HNLC waters (Kopczyńska et al.,  
11 1998; Gall et al., 2001). Similar results were reported for the HNLC station of the first cruise  
12 KEOPS1 (Uitz et al., 2009).

#### 13 4.2.2 The iron-fertilized stations

14 By contrast, larger developments of phytoplankton were observed in the iron-fertilized  
15 Kerguelen region, confirming the classical stimulation of phytoplankton growth under iron-  
16 replete conditions (Martin, 1990). Integrated chlorophyll biomass (152.5 ± 77.4 mg m<sup>-2</sup>;  
17 Fig. 2a and 7) fell in the range typically reported for different regions of the Southern Ocean  
18 (Peeken, 1997; Wright and van den Enden, 2000; Uitz et al., 2009). Some very high  
19 productive stations (A3-2, E-4W2 and the area from TEW-7 to TEW-8) were comparable to  
20 the highly productive regions like the Ross sea (Goffart et al., 2000), reflecting the high  
21 productivity of the early bloom. The large development of diatoms was notably evidenced at  
22 station A3 where Chl *a* biomass increased 3.5-fold from October to November.

23 All over the iron-fertilized area, chlorophyll biomass was largely dominated by large diatoms  
24 (> 20 μm; Fig. 2b and 7), as suggested by the higher concentrations in fucoxanthin over the  
25 other pigments. Previous artificial iron-fertilization experiments reported the shift from nano-  
26 and/or picophytoplanktonic communities to large diatoms (> 20 μm) after Fe-addition (Gall et  
27 al., 2001; Hoffmann et al., 2006; Lance et al., 2007). The dominance of large diatoms was  
28 also observed in other natural Fe-fertilized regions of the Southern Ocean (Bathmann et al.,  
29 1997; Moore et al., 2007; Uitz et al., 2009).

30 Interestingly, relatively high Chl *a* biomasses were found below the mixed layer all over the  
31 iron-fertilized area. This feature was also observed during KEOPS1 at the Plateau reference

1 station A3 and resulted in the progressive formation of a deep chlorophyll maximum (DCM)  
2 associated to a deep biogenic silica maximum at 125 m (Mosseri et al., 2008; Uitz et al.,  
3 2009). Uitz et al. (2009) explained this DCM by the accumulation of inactive but living algal  
4 cells at the deep temperature-driven pycnocline. During KEOPS2, a second density gradient  
5 (identified from the  $\sigma_\theta$  profiles) deeper than the MLD was observed for most of the stations  
6 over the iron-fertilized area. Furthermore, Si-production by diatoms was lower but still  
7 observed below the mixed layer although irradiance levels were  $< 1\%$  PAR  
8 (Photosynthetically Active Radiation; Closset et al., this issue; Lasbleiz et al., in prep.). The  
9 acclimation of phytoplankton to low light levels has already been reported by Cullen (1982)  
10 and more recently by Banse (2004) and Marra et al. (2014). In addition, cell counts revealed  
11 that the community composition was rather the same within and beneath the mixed layer, with  
12 the difference that the proportion of empty cells was higher beneath the mixed layer. These  
13 observations would suggest that Chl *a* biomass below the mixed layer would result from the  
14 sedimentation of living diatoms from the upper layer rather than *in situ* growth of a specific  
15 deep-dwelling community. Characterized by low light levels and high nutrient  
16 concentrations, the layer between the surface mixed layer and the second pycnocline would  
17 also allow a slight growth of phytoplankton. Thereafter, this accumulation of sinking cells  
18 could be enhanced by the shift of phytoplankton communities towards more heavily silicified  
19 diatoms, observed later in the season by Armand et al. (2008). Together all these observations  
20 could explain the occurrence of the DCM observed at the Plateau reference station A3 during  
21 the demise of the bloom (Uitz et al., 2009).

## 22 **4.3 Element composition and stoichiometry**

### 23 **4.3.1 Si, C, N, P stocks**

24 Above 200 m, the iron-fertilized stations were characterized by the progressive development  
25 of micro-sized diatoms ( $> 20\ \mu\text{m}$ ) resulting in high biogenic silica and particulate organic  
26 matter concentrations at some productive stations (A3-2, E-4W2, and the area from TEW-7 to  
27 TEW-8; Fig. 8 and 12). These high concentrations fell in the range of those measured in the  
28 PFZ in spring (Quéguiner et al., 1997; Brzezinski et al., 2001; Quéguiner and Brzezinski,  
29 2002). At the HNLC reference station, BSi stocks were clearly lower due to a higher  
30 proportion of nanoflagellates (39 %).

1 Below 200 m, the biogenic silica (especially at A3, E-4W, TEW-7 and TEW-8) was  
2 dominated by the smaller (0.8 to 20  $\mu\text{m}$ ) size fraction despite the development of large  
3 diatoms in surface waters (Fig. 11 and 12). This could either reflect the sedimentation of  
4 small diatoms coming from a short bloom event before sampling or/and an active degradation  
5 of diatoms at the top of the mesopelagic zone inducing the fragmentation of siliceous  
6 planktonic particles by grazers. Given that organic matter is preferentially degraded relative to  
7 biogenic silica, the hypothesis of an enhanced degradation from 200 m and beyond could  
8 explain the low POC export reported by Planchon et al. (this volume) who also report  
9 elevated  $^{234}\text{Th}:$  $^{238}\text{U}$  ratios slightly  $> 1$  in between 250 and 700 m at E-3 and in between 200 to  
10 600 m at E-5. Similarly, Jacquet et al. (this volume) report a  $\text{Ba}_{\text{xs}}$  maximum centered around  
11 400 m at E-3 and E-5 which indicates an increased remineralisation of organic matter. From  
12 various sediment trap deployments at 200 m depth, Laurenceau et al. (this volume) evidenced  
13 a negative correlation between primary productivity and export efficiency, suggesting that the  
14 highest productive stations were the least efficient to carbon export.

#### 15 4.3.2 Elemental stoichiometry Si:C, Si:N and Si:P in particulate matter

16 Both artificial and natural iron-fertilization experiments have documented the influence of  
17 iron on the elemental ratios of phytoplankton communities (Hutchins and Bruland, 1998;  
18 Takeda, 1998; Franck et al., 2000; Hare et al., 2007; Moore et al., 2007). They usually  
19 mention higher (2 to 3 times) Si:C, Si:N and Si:P ratios under Fe-stress as compared to values  
20 under Fe-replete conditions (Si:C = 0.13, Si:N = 1.1; Brzezinski, 1985). This is supposed to  
21 indicate the development of more heavily silicified diatoms under iron-stress (Hutchins and  
22 Bruland, 1998; Takeda, 1998). Surprisingly, we report here an opposite trend (Fig. 13): the  
23 iron-fertilized stations mentioned above evidenced 2-fold higher Si:C and Si:N ratios than  
24 those of the HNLC station R2 (close to Brzezinski's ratios). The high Si:C and Si:N ratios  
25 observed at the iron-fertilized stations could be explained by a differential recycling of  
26 organic matter and biogenic silica, increased Si requirements by the dominant species and/or  
27 the presence of empty cells. Bacterial activity and grazing pressure by zooplankton could  
28 explain the preferential degradation of soft organic matter over BSi dissolution in surface  
29 waters. However, in the early productive period, their impact on particulate matter  
30 stoichiometry is probably not yet significant: Christaki et al. (this volume) indicates that a few  
31 percent of primary production (gross community production; Cavagna et al., this volume) at

1 A3 are channeled through the microbial loop and the mesozooplankton. Furthermore,  
2 countings revealed that the numbers of empty cells were very low compared to living cells at  
3 the iron-fertilized stations (Lasbleiz et al., in prep.), which could not explain such high  
4 Si:C/N/P ratios.

5 The high Si:C, Si:N and Si:P ratios of the productive stations would then rather indicate the  
6 presence of phytoplankton communities dominated by heavily silicified diatoms. Our  
7 interpretation agrees with the high Si uptake rates, compared to C and N uptake rates,  
8 measured at A3, E-4W and F-L (located between TEW-7 and TEW-8) by Closset et al. (this  
9 volume). These results are consistent with Si:C production ratios reported for the PFZ during  
10 austral spring and reaching values as high as 0.45 in the Pacific sector (Brzezinski et al.,  
11 2001) and 0.32 to 1.19 in the Atlantic sector (Quéguiner and Brzezinski, 2002). However,  
12 while these authors attribute the strong silicification to limitation by iron, it seems, in our  
13 instance, that the ratios we observe during the early blooms are rather related to the taxonomic  
14 composition of diatom assemblages. It is interesting to notice that the highest Si:C ratio of  
15 1.19, reported by Quéguiner and Brzezinski (2002), was observed during the early stage of a  
16 bloom development dominated by *Corethron criophilum* and *Fragilariopsis kerguelensis*, and  
17 that the Si:C ratio then decreased to the lower value of 0.32 later in the season. Our  
18 observations would thus suggest that biogenic particulate matter at the onset of the blooms of  
19 naturally iron-fertilized environments could be typically Si enriched compared to C, N and P,  
20 due to the presence of specific diatom communities. Our finding is a major difference  
21 between the experiments of natural fertilization and artificial fertilization in the Southern  
22 Ocean. In the latter, diatoms that grow are often referred to as opportunistic species such as  
23 *Pseudo-Nitzschia* spp. and *Chaetoceros* spp. and these taxa are also those involved in the  
24 pioneer works of Hutchins and Bruland (1998) and Takeda (1998). Apart from this general  
25 trend, the European Iron Fertilisation Experiment (EIFEX) did not evidence the classical  
26 decrease of Si:C and Si:N ratios observed in artificial iron-experiments (Hoffmann et al.,  
27 2006; Smetacek et al., 2012). Initial Si:C, Si:N and Si:P elemental ratios (respectively 0.24,  
28 1.5 and 18.0) increased from 1.8 to 2.6 times in 37 days after the first fertilization. This  
29 feature was attributed to a shift, more pronounced compared to the other artificial fertilization  
30 studies, towards more heavily silicified diatom species. Furthermore, the laboratory cultures  
31 of two Southern Ocean diatom species (*Fragilariopsis kerguelensis* and *Chaetoceros*  
32 *dichaeta*) highlighted the species-specific response to iron availability in the elemental



1 composition (Hoffmann et al., 2007). Under natural conditions, the control of stoichiometric  
2 ratios is thus more complex and depends largely on the diatom community structure, itself  
3 depending on the dominant species adapted to their specific set of environmental conditions.

4 Although surprising at first sight, the low Si:C and Si:N ratios observed at R2 (Fig. 13) are  
5 explained by the dominance of non-siliceous organisms (mostly nanoflagellates) decreasing  
6 Si proportion compared to C and N in the bulk particulate matter. Diatoms contribution to C  
7 biomass was however significant (representing 34 % of the particulate organic carbon at the  
8 surface; Lasbleiz et al., in prep.) which could reflect a short development of a diatom  
9 assemblage just prior our sampling. This is consistent with the high dissolution rates of BSi  
10 observed in surface waters (Closset et al., this volume) and the high mineralization activity  
11 evidenced in the mesopelagic zone (Jacquet et al., this volume). It is likely that particular  
12 biogeochemical conditions characterizing the start of the productive period would have  
13 induced a progressive shift in the community composition. At the end of winter, the reference  
14 station R2 would be characterized by high-nutrient waters, and unfavorable light conditions  
15 for diatom growth. By early spring, iron concentrations were relatively low but likely  
16 sufficient to trigger a short phytoplankton growth as soon as light conditions became  
17 favorable. Given the low iron winter stock available, the bloom quickly stops well before the  
18 diatoms have had time to use the stock of macronutrients. This would induce optimal  
19 conditions to the development of heterotrophic communities, able to grow on the decaying  
20 bloom of diatoms.

#### 21 4.3.3 Elemental stoichiometry C:N, C:P and N:P in organic particulate matter

22 During KEOPS2, we observed a consistently lower N:P ratio compared to the canonical  
23 Redfield ratio of 16 (Fig. 13). Moreover, among the different stations, the cluster of  
24 productive stations located north of the PF had a significantly lower average N:P ratio  
25 ( $10.5 \pm 3.3$ ) than all other clusters ( $> 11$ ). Indeed the N:P ratio is highly variable in  
26 phytoplankton (Geider and La Roche, 2002) and tends to be lower than 16 in nutrient-replete  
27 cultures of phytoplankton. Klausmeier et al. (2004) showed that the optimal phytoplankton  
28 stoichiometry varied, with  $N:P < 16$  associated with phytoplankton growing exponentially and  
29  $N:P > 16$  at competitive equilibrium. For diatoms, Sarthou et al. (2008) have reported an  
30 average ratio of  $10 \pm 4$ , based on the review of available literature. In the field, N:P ratios vary  
31 also widely (Martiny et al., 2013) and low values have been reported in association to the

1 dominance of diatoms (Arrigo et al., 2002). Our observations of low N:P ratios are consistent  
2 with the dominance of diatoms in the KEOPS2 region. The lowest N:P ratio in the most  
3 productive region is also confirmed by the temporal evolution of nitrate and phosphate  
4 distributions which show a preferential drawdown of phosphate in this region (Blain et al.,  
5 this volume).

6 Ecophysiological studies of the effect of iron limitation on phytoplankton elemental ratio has  
7 led to different and somewhat contradictory results. The results of Price (2005) with  
8 *Thalassiosira weissflogii* suggested that iron limitation leads to a decreased N:P ratio.  
9 However Hoffman et al. (2007) working with *Fragilariopsis kerguelensis* and *Chaetoceros*  
10 *dichaeta* did not observe any change in C/N/P ratios in relation to iron limitation. During  
11 EIFEX, the initial N:P ratios and their evolution as the bloom developed were very different  
12 for two different size classes (Hoffmann et al., 2006). For the microphytoplankton (> 20 µm),  
13 N:P was < 16 before fertilization and increased as the iron fertilized bloom developed. For  
14 nanoplankton (2 µm to 20 µm) the opposite trend was observed: the initial N:P ratio was close  
15 to 16 and decreased in the course of the bloom. In the case of the natural iron fertilization  
16 around Kerguelen, we also observed a large variability between stations. But large changes  
17 have also been documented at the seasonal scale. N:P of  $17 \pm 2$  was measured in March  
18 (Copin-Montegut and Copin-Montegut, 1978) at stations east of the Kerguelen Islands that  
19 were close to the cluster of stations E. All these results suggest that the variability of N:P  
20 ratios occurring in response to iron fertilization is ecologically driven. How these changes  
21 translated in the N and P elemental composition of sinking particulate matter would certainly  
22 deserve further studies.

23 The C:N ratio was close to the Redfield ratio only at the HNLC station (Fig. 13). For all other  
24 stations, the C:N ratio was significantly lower but without any difference between the  
25 different clusters of stations. This confirms that the C:N ratio is generally not largely affected  
26 by iron limitation (Price, 2005; Hoffmann et al., 2007). Low values were previously reported  
27 in the Southern Ocean including the Kerguelen region (Copin-Montegut and Copin-Montegut,  
28 1978; Tréguer et al., 1988). This was considered as a general feature of the iron limited  
29 Southern Ocean and interpreted as an excess of P accumulation during Fe-limited growth of  
30 phytoplankton (Price, 2005). Hoffmann et al. (2006) also observed low C:P ratios in HNLC  
31 waters of the Atlantic sector of the Southern Ocean, with only a modest increase in response  
32 to iron fertilization. Our results from KEOPS2 also report low C:P ratios in response to iron

1 fertilization (Fig. 13). However similarly to what was discussed above for N:P, C:P increased  
2 to values close to the Redfield ratio at the end of the season (Copin-Montegut and Copin-  
3 Montegut, 1978).

4 In the Southern Ocean, iron limitation and iron fertilization may favor P accumulation in  
5 phytoplankton for different physiological or ecological reasons, leading to N:P and C:P lower  
6 than Redfield ratios. However this conclusion based on average values may hide differences  
7 especially on temporal scales that are not resolved by the resolution of this data set. Overall,  
8 our results also confirm a tendency of a decrease of C:N:P ratios in nutrient-rich high latitude  
9 waters highlighted by Martiny et al. (2013) by comparison with warmer oligotrophic or  
10 upwelling areas.

#### 11 4.3.4 Seasonal evolution of Si, C and N cycles at the southeast plateau bloom

12 The KEOPS program provides information on the biogeochemical functioning of the  
13 southeastern KP at two different periods of the seasonal cycle: the early spring (October-  
14 November, 2011 - KEOPS2) and the late summer (January-February, 2005 - KEOPS1).  
15 Combining the two data sets at station A3 gives us the first opportunity to describe the  
16 seasonal evolution of Si, C and N cycles under natural iron fertilization in relation to  
17 community composition.

18 During the KEOPS2 cruise, the first visit at A3 (October 20, A3-1) was characteristic of early  
19 bloom conditions. Low biogenic and particulate organic matter concentrations were observed  
20 despite high nutrients (Blain et al., this volume) and iron concentrations (Bowie et al., this  
21 volume) as well as a low mesozooplankton grazing pressure (Carlotti et al., this volume).  
22 Phytoplankton growth was most likely limited by low irradiance levels as expected in winter  
23 and early spring (Boyd, 2002). Integrated elemental ratios (over 200 m) were close to the  
24 canonical ratios of Redfield et al. (1963) and Brzezinski et al. (1985), reaching values of 0.13  
25 for Si:C, 1.2 for Si:N, 16.9 for Si:P, 9.0 for C:N, 128.7 for C:P and 14.3 for N:P.

26 At the second visit (November, 16), a large development of diatoms was observed above the  
27 KP due to more favorable light conditions. Biogenic silica and particulate organic matter  
28 concentrations were at least 2 fold higher than in October (713.3 mmol Si m<sup>-2</sup> for BSi,  
29 2,267 mmol C m<sup>-2</sup> for POC, 435.9 mmol N m<sup>-2</sup> for PON, and 29.3 mmol P m<sup>-2</sup> for POP) and  
30 Si production fluxes were among the highest reported so far in the Southern Ocean (47.9  
31 mmol Si m<sup>-2</sup> d<sup>-1</sup>; Closset et al., this issue). Si:C and Si:N ratios (respectively 0.31 and 1.6)

1 were higher than Brzezinski's ratios (1985). This could directly result from the high Si:C and  
2 Si:N uptake ratios (respectively 0.30 and 1.5) reported by Closset et al. (this volume) which  
3 were remarkably close to our stock ratios, meaning that it is a characteristic of the species  
4 growing in our study area. At this period, the organic carbon produced would be transferred to  
5 small zooplankton populations which in turn would feed the large zooplankton population  
6 (Henjes et al., 2007). The C budget of Christaki et al. (this volume) however, indicates that an  
7 overall small fraction of primary production is transferred to higher trophic levels. Added to  
8 the low vertical export of C reported by Planchon et al. (this volume), both observations are  
9 strong arguments of biogenic matter retention in the surface mixed layer at the beginning of  
10 the KP bloom.

11 During the KEOPS1 cruise, the period from 19<sup>th</sup> January to 12<sup>th</sup> February corresponded to the  
12 last active stage of the productive period. At the start of the cruise, an unusually high level of  
13 BSi had already accumulated ( $2,105 \text{ mmol Si m}^{-2}$ ) in the mixed layer which progressively  
14 declined until February (Mosseri et al., 2008). The C:N ratios of particulate matter were  
15 higher than in November, and increased with depth, ranging from 6.7 at the surface to 8.7 at  
16 129 m (Trull et al., 2008). This was attributed to the increase of POC concentrations with  
17 depth, likely induced by settling of the increasingly senescent diatom bloom over the plateau  
18 (Mosseri et al., 2008; Trull et al., 2008). Si:C and Si:N uptake ratios were close to 0.13 and 1.  
19 However, the high  $\text{NO}_3^-$  concentrations in surface waters compared to  $\text{H}_4\text{SiO}_4$  depletion at the  
20 end of the bloom suggested a strong decoupling between the seasonal consumption of these  
21 two nutrients. This could be due to differential remineralisation rates between Si and N, as  
22 evidenced by elevated concentration of ammonium, and by the ability of diatoms to grow on  
23 ammonium as nitrogen source (Mosseri et al., 2008). The system would thus behave as a  
24 strong silicon pump favoring Si export to deep waters compared to N. A decoupling between  
25 C and N cycles was also hypothesized: high amounts of exported C were reported evidencing  
26 a strong biological pump of C (Mosseri et al., 2008; Trull et al., 2008). So, the end of the  
27 productive period would be associated to the main event of massive export of biogenic silica  
28 and organic matter as proposed by Quéguiner (2013). This feature seems coherent when  
29 comparing the most abundant diatom species found in surface waters at the end of the  
30 productive period and those found in sediment thanatocoenoses. Indeed, *Eucampia antarctica*  
31 and *Chaetoceros* resting spores were the dominant species both in surface waters and in the

1 sediments (Armand et al., 2008; Wilks, 2013) suggesting enhanced export of particulate  
2 matter at the end of the productive period.

#### 3 **4.4 LSi as tracer of lithogenic matter transport?**

4 All over the study area (Fig. 14 and 15), LSi concentrations fell in the same range of values  
5 previously measured in the Southern Ocean, both in the PFZ (Quéguiner et al., 1997;  
6 Quéguiner, 2001; Leblanc et al., 2002) and the POOZ (Quéguiner et al., 1997; Bucciarelli et  
7 al., 2001). TNS-1 and R2 stations showed low LSi concentrations typically observed for  
8 regions far from continental influence ( $< 0.04 \mu\text{mol L}^{-1}$ ; Leblanc et al., 2002). Surprisingly, a  
9 local maximum was reported at 500 m at station R2, reflecting particulate lithogenic inputs at  
10 depth. A similar pattern was found for particulate and dissolved trace metals (Bowie et al.,  
11 this volume; Quéroué et al., this volume; van der Merwe et al., this volume). In these studies,  
12 lateral transport of lithogenic matter from the Leclaire Rise, a large seamount located west of  
13 station R2, was hypothesized to explain this local maximum.

14 In contrast to R2 and TNS-1, two regions were characterized by very high LSi concentrations  
15 typically reported for regions subjected to continental influence (Bucciarelli et al., 2001): the  
16 coastal waters over the entire water column (TEW-1 to TEW-3) and the reference plateau  
17 station A3 near the bottom. For the coastal waters (TEW-1 to TEW-3), LSi could come from  
18 multiple lithogenic sources such as soil erosion, riverine discharges or aeolian inputs  
19 (Bucciarelli et al., 2001). At A3, the maximum concentration near the bottom would rather  
20 reflect sediment resuspension in the water column. Another striking feature at A3 was the  
21 relatively high concentrations from the surface down to 300 m. Two potential sources of  
22 lithogenic material could explain these higher concentrations: LSi could come from below  
23 due to an elevated vertical mixing or from the extensive shoal around the Heard/Mc Donald  
24 Islands by horizontal advection (Blain et al., 2007; Park et al., 2008a). Interestingly,  
25 maximum concentrations were found at 400 m for E-4W2 and between 600 and 700 m at the  
26 different visits of the complex system of recirculation (stations E). This could evidence lateral  
27 transport of LSi-rich waters coming from the plateau and more likely from the Heard/Mc  
28 Donald Islands in the case of E-4W. Our results were consistent with the study of Bowie et al.  
29 (this volume) which reported lithogenic particulate iron coming from the plateau between 400  
30 and 600 m at E-1, E-3 and E-5.

1 In the PF area (from TEW-7 to TEW-8), relatively higher concentrations compared to  
2 surrounding waters ( $> 0.11 \mu\text{mol L}^{-1}$ ) were observed over the water column. Such a pattern  
3 was already reported by previous studies in different sectors of the Southern Ocean  
4 (Quéguiner et al., 1997; Bucciarelli et al., 2001). At the southern border of the PFZ in the  
5 Atlantic sector, high LSi concentrations were associated to local inputs from atmospheric  
6 deposition. By using the NOAA HYSPLIT 1-day and 5-day backward trajectory atmospheric  
7 model, no atmospheric inputs were evidenced as suggested by the absence of air masses  
8 flowing over the eastern area north of the PF (Quérroué et al., this volume). However,  
9 considering that no direct measurements of dust deposition were performed during KEOPS2,  
10 the hypothesis of aeolian inputs cannot be completely rejected. In addition, a recent study  
11 performed in the Kerguelen region demonstrated that atmospheric deposition fluxes have  
12 been underestimated until now (Heimbürger et al., 2012). Both aeolian inputs and lateral  
13 advection of LSi-rich waters could thus explain the relatively higher concentrations between  
14 TEW-7 and TEW-8. LSi-rich waters would probably result from the northwest transport of  
15 deep waters from the KP (Zhou et al., this volume) or from the mixture of the advected  
16 coastal waters with the subantarctic water (Bucciarelli et al., 2001). The station TNS-2,  
17 located north of the PF, would also suggest aeolian dust deposition coupled with lateral  
18 advection of LSi-rich waters by evidencing local LSi maximums at the surface and  
19 subsurface.

20 By comparing particulate iron and other trace metal distribution (Bowie et al., this volume),  
21 similar patterns were observed at R2, A3 and E stations over the water column. This suggests  
22 that LSi would be a good tracer to track lithogenic material inputs (and indirectly iron) from  
23 aeolian transport, terrestrial erosion as well as sediment resuspension to the water column. All  
24 the more so that the Kerguelen Islands are mainly composed of flood basalt, a Si-rich rock  
25 (Gautier, 1987). In this study, several potential sources were mentioned to explain the  
26 distribution of lithogenic matter all over the study area. The northward transport of lithogenic  
27 matter and vertical transport from deep waters enriched in lithogenic materials were expected  
28 from the KEOPS1 study (Blain et al., 2007; van Beek et al., 2008; Park et al., 2008a).  
29 Furthermore, even if the contribution of atmospheric inputs is still matter of debate (Cassar et  
30 al., 2007; Heimbürger et al., 2012), dust deposition could play a significant role in supplying  
31 lithogenic matter in the Kerguelen region.

## 1 **5 Conclusions**

2 The distribution of particulate matter and phytoplankton community structure above the  
3 natural iron-fertilized Kerguelen region was strongly impacted by the complex mesoscale  
4 structure of water masses, generated by the interaction between the KP topography and the  
5 Polar Front pathway. In early spring, the eastern side of the KP was characterized by a mosaic  
6 of biogeochemical situations that could be divided into five contrasted environments. A  
7 productive coastal area was first isolated by a shelf break front from a second area less  
8 productive corresponding to a cold water tongue circulating northward and likely limited by  
9 light availability. The situation was different in the meander of the PF, where the complex  
10 mesoscale activity induced a phytoplankton development delayed by comparison to the KP  
11 itself. Two high productive areas were located at the easternmost study area north in the PF  
12 and over the southeastern KP where light conditions and nutrients (including iron) availability  
13 were favorable to phytoplankton growth. Biogeochemical properties of the eastern flank of  
14 the KI supports the idea that the extensive bloom of the southeastern KP was, at least partly,  
15 advected northwards.

16 The comparison between the iron-fertilized productive sites and the iron-limited HNLC area  
17 showed that iron stimulated the accumulation of large ( $> 20\mu\text{m}$ ) siliceous particulate matter at  
18 the onset of the bloom. Under iron stress, the low Si biomass was mainly associated to mixed,  
19 nanoflagellate-dominated, phytoplankton population but Si:C:N:P ratios were unexpectedly  
20 close to the typical values for nutrient-replete diatoms, which was likely due to the presence  
21 of siliceous detritus from an earlier bloom. In the iron-fertilized areas, we showed a patchy  
22 response of particulate matter distribution and stoichiometric ratios but with overall elevated  
23 Si:C:N:P. This suggests the presence of heavily silicified diatoms contrary to the classical  
24 paradigm of Hutchins & Bruland (1998) and Takeda (1998). The variable and patchy nature  
25 of responses in the natural surroundings of the KI calls for cautious consideration in  
26 extrapolating the results from artificial iron fertilization experiments.

27 The seasonal evolution of the bloom over the southeastern KP (A3 station) is characterized by  
28 a progressive evolution of the Si:C:N ratios and the phytoplankton community composition  
29 probably resulting in different export regimes at the beginning (retention in the ML) and the  
30 end of the productive season (massive vertical export). At the onset of the bloom, the weak  
31 vertical export, mainly driven by nanoplanktonic size fraction of biogenic silica, could be the

1 result of the fragmentation of particles originating from aborted late winter blooms. Given the  
2 high Si:C:N ratios in the surface waters and the expected preferential degradation of organic  
3 matter by small zooplankton community in the course of the productive period, the system  
4 behaves as a moderate silicon pump in spring. At the end of the bloom, the increasing  
5 influence of silicic acid depletion and changes in the phytoplankton community structure  
6 result in decreased Si:C and Si:N ratios. Additionally, increased grazing pressure from  
7 mesozooplankton leads to a massive export of biogenic silica and carbon organic matter at  
8 depth which occurs later in the season (Rembauville et al., in prep.). In the natural iron  
9 fertilized Kerguelen region, understanding the patchy development of distinct blooms with  
10 varying Si:C:N:P composition and the ultimate fate of produced biogenic silica and organic  
11 carbon (as in the “silica-sinkers” vs “carbon-sinkers” hypothesis; Assmy et al., 2013) calls for  
12 a finer characterization of diatoms interspecific contribution to both Si production and C  
13 biomass, which can only be addressed by taxonomic studies and cellular labelling (Lasbleiz et  
14 al., in prep.). As emphasized by Boyd (2013), the concept of functional group tends to fall  
15 short when probing its responses to environmental forcings and diatom floristic shifts impact  
16 on global biogeochemical cycles needs to be further understood.

17

## 18 **Acknowledgements**

19 We thank the captain Bernard Lassiette and crew of the R/V Marion Dufresne for their  
20 support aboard. We also thank M. Ouhssain from the French SAPIGH analytical platform for  
21 pigment sampling and analysis. We thank A.C Martiny and an anonymous referee for their  
22 constructive comments. This work was supported by the French Research program of INSU-  
23 CNRS LEFE–CYBER (‘Les enveloppes fluides et l’environnement’ – ‘Cycles  
24 biogéochimiques, environnement et ressources’), the French ANR (‘Agence Nationale de la  
25 Recherche’, SIMI-6 program), the French CNES (‘Centre National d’Etudes Spatiales’) and  
26 the French Polar Institute IPEV (Institut Polaire Paul–Emile Victor).

27



## 1 **References**

- 2 Armand, L. K., Cornet-Barthaux, V., Mosseri, J., and Quéguiner, B.: Late summer diatom  
3 biomass and community structure on and around the naturally iron-fertilised Kerguelen  
4 Plateau in the Southern Ocean, *Deep Sea Research Part II: Topical Studies in Oceanography*,  
5 55, 653-676, 10.1016/j.dsr2.2007.12.031, 2008.
- 6 Armstrong, R. A., Peterson, M. L., Lee, C., and Wakeham, S. G.: Settling velocity spectra and  
7 the ballast ratio hypothesis, *Deep Sea Research Part II: Topical Studies in Oceanography*, 56,  
8 1470-1478, 10.1016/j.dsr2.2008.11.032, 2009.
- 9 Arrigo, K. R., Dunbar, R. B., Lizotte, M. P., and Robinson, D. H.: Taxon-specific differences  
10 in C/P and N/P drawdown for phytoplankton in the Ross Sea, Antarctica, *Geophysical*  
11 *Research Letters*, 29, 1938, 10.1029/2002gl015277, 2002.
- 12 Arrigo, K. R., and Alderkamp, A.-C.: Shedding dynamic light on Fe limitation (DynaLiFe),  
13 *Deep Sea Research Part II: Topical Studies in Oceanography*, 71-76, 1-4,  
14 10.1016/j.dsr2.2012.03.004, 2012.
- 15 Assmy, P., Smetacek, V., Montresor, M., Klaas, C., Henjes, J., Strass, V. H., Arrieta, J. M.,  
16 Bathmann, U., Berg, G. M., Breitbarth, E., Cisewski, B., Friedrichs, L., Fuchs, N., Herndl, G.  
17 J., Jansen, S., Krägfesky, S., Latasa, M., Peeken, I., Rüttgers, R., Scharek, R., Schüller, S. E.,  
18 Steigenberger, S., Webb, A., and Wolf-Gladrow, D.: Thick-shelled, grazer-protected diatoms  
19 decouple ocean carbon and silicon cycles in the iron-limited Antarctic Circumpolar Current,  
20 *Proceedings of the National Academy of Sciences, USA*, 110, 20633-20638, 2013.
- 21 Banse, K.: Should we continue to use the 1% light depth convention for estimating the  
22 compensation depth of phytoplankton for another 70 years?, *Limnology and Oceanography*  
23 *Bulletin*, 13, 49-51, 2004.
- 24 Bathmann, U. V., Scharek, R., Klaas, C., Dubischar, C. D., and Smetacek, V.: Spring  
25 development of phytoplankton biomass and composition in major water masses of the  
26 Atlantic sector of the Southern Ocean, *Deep Sea Research Part II: Topical Studies in*  
27 *Oceanography*, 44, 51-67, 10.1016/S0967-0645(96)00063-X, 1997.
- 28 Blain, S., Tréguer, P., Belviso, S., Bucciarelli, E., Denis, M., Desabre, S., Fiala, M., Martin  
29 Jézéquel, V., Le Fèvre, J., Mayzaud, P., Marty, J.-C., and Razouls, S.: A biogeochemical  
30 study of the island mass effect in the context of the iron hypothesis: Kerguelen Islands,  
31 Southern Ocean, *Deep Sea Research Part I: Oceanographic Research Papers*, 48, 163-187,  
32 10.1016/S0967-0637(00)00047-9, 2001.
- 33 Blain, S., Queguiner, B., Armand, L., Belviso, S., Bombled, B., Bopp, L., Bowie, A., Brunet,  
34 C., Brussaard, C., Carlotti, F., Christaki, U., Corbiere, A., Durand, I., Ebersbach, F., Fuda, J.-  
35 L., Garcia, N., Gerringa, L., Griffiths, B., Guigue, C., Guillerm, C., Jacquet, S., Jeandel, C.,  
36 Laan, P., Lefevre, D., Lo Monaco, C., Malits, A., Mosseri, J., Obernosterer, I., Park, Y.-H.,  
37 Picheral, M., Pondaven, P., Remenyi, T., Sandroni, V., Sarthou, G., Savoye, N., Scouarnec,  
38 L., Souhaut, M., Thuiller, D., Timmermans, K., Trull, T., Uitz, J., van Beek, P., Veldhuis, M.,  
39 Vincent, D., Viollier, E., Vong, L., and Wagener, T.: Effect of natural iron fertilization on

- 1 carbon sequestration in the Southern Ocean, *Nature*, 446, 1070-1074, 10.1038/nature05700,  
2 2007.
- 3 Blain, S., Oriol, L., Capparos, J., Guéneuguès, A., and Obernosterer, I.: Distributions and  
4 stoichiometry of dissolved nitrogen and phosphorus in the iron fertilized region near  
5 Kerguelen (Southern Ocean), *Biogeosciences KEOPS 2 special issue*, this volume.
- 6 Bowie, A. W., van der Merwe, P., Trull, T., Quéroué, F., Fourquez, M., Planchon, F.,  
7 Sarthou, G., and Blain, S.: Iron budgets for three distinct biogeochemical sites around the  
8 Kerguelen plateau (Southern Ocean) during the natural fertilization experiment KEOPS-2,  
9 *Biogeosciences KEOPS 2 special issue*, this volume.
- 10 Boyd, P. W., LaRoche, J., Gall, M., Frew, R., and McKay, R. M. L.: Role of iron, light, and  
11 silicate in controlling algal biomass in subantarctic waters SE of New Zealand, *Journal of*  
12 *Geophysical Research: Oceans*, 104, 13395-13408, 10.1029/1999jc900009, 1999.
- 13 Boyd, P. W.: Environmental factors controlling phytoplankton processes in the Southern  
14 Ocean, *Journal of Phycology*, 38, 844-861, 10.1046/j.1529-8817.2002.t01-1-01203.x, 2002.
- 15 Boyd, P. W.: Biogeochemistry: Iron findings, *Nature*, 446, 989-991, 10.1038/446989a, 2007.
- 16 Boyd, P. W.: Diatom traits regulate Southern Ocean silica leakage, *Proceedings of the*  
17 *National Academy of Sciences*, 110, 20358-20359, 10.1073/pnas.1320327110, 2013.
- 18 Brzezinski, M. A.: The Si:C:N ratio of marine diatoms: interspecific variability and the effect  
19 of some environmental variables, *J. Phycol.*, 21, 347-357, 1985.
- 20 Brzezinski, M. A., Nelson, D. M., Franck, V. M., and Sigmon, D. E.: Silicon dynamics within  
21 an intense open-ocean diatom bloom in the Pacific sector of the Southern Ocean, *Deep Sea*  
22 *Research Part II: Topical Studies in Oceanography*, 48, 3997-4018, 10.1016/S0967-  
23 0645(01)00078-9, 2001.
- 24 Bucciarelli, E., Blain, S., and Tréguer, P.: Iron and manganese in the wake of the Kerguelen  
25 Islands (Southern Ocean), *Marine Chemistry*, 73, 21-36, 10.1016/S0304-4203(00)00070-0,  
26 2001.
- 27 Buesseler, K. O.: The decoupling of production and particulate export in the surface ocean,  
28 *Global Biogeochemical Cycles*, 12, 297-310, 10.1029/97gb03366, 1998.
- 29 Cailliau, C., Claustre, H., and Giannino, S.: Chemotaxonomic analysis of phytoplankton  
30 distribution in the Indian sector of the Southern Ocean during late austral summer, *Oceanologica*  
31 *Acta*, 20, 721-732, 1997.
- 32 Carlotti, F., Nowaczyk, A., Jouandet, M.-P., Lefèvre, D., and Harmelin, M.:  
33 Mesozooplankton structure and functioning during the onset of the Kerguelen bloom during  
34 KEOP2 survey, *Biogeosciences KEOPS 2 special issue*, this volume.
- 35 Cassar, N., Bender, M. L., Barnett, B. A., Fan, S., Moxim, W. J., Levy, H., and B., T.: The  
36 southern ocean biological response to aeolian iron deposition, *Science*, 317, 1067-1070,  
37 10.1126/science.1144602, 2007.

- 1 Cavagna, A. J., Lefèvre, D., Dehairs, F., Elskens, M., Fripiat, F., Closset, I., Lasbleiz, M.,  
2 Flores-Leive, L., Cardinal, D., Leblanc, K., Fernandez, C., Oriol, L., Blain, S., and Quéguiner,  
3 B.: Biological productivity regime in the surface waters around the Kerguelen Island in the  
4 Southern Ocean - from the use of an integrative approach, Biogeosciences KEOPS 2 special  
5 issue, this volume.
- 6 Christaki, U., Lefèvre, D., Georges, C., Colombet, J., Catala, P., Sime-Ngando, T., Blain, S.,  
7 and Obernosterer, I.: Microbial food web dynamics during spring phytoplankton blooms in  
8 the naturally iron-fertilized Kerguelen area (Southern Ocean), Biogeosciences KEOPS 2  
9 special issue, this volume.
- 10 Claustre, H.: The trophic status of various oceanic provinces as revealed by phytoplankton  
11 pigment signatures, *Limnology and Oceanography*, 39, 1206-1210,  
12 10.4319/llo.1994.39.5.1206, 1994.
- 13 Closset, I., Lasbleiz, M., Leblanc, K., Quéguiner, B., Cavagna, A.-J., Elskens, M., Navez, J.,  
14 and Cardinal, D.: Seasonal evolution of net and regenerated silica production around a natural  
15 Fe-fertilized area in the Southern Ocean estimated from Si isotopic approaches,  
16 Biogeosciences KEOPS 2 special issue, this volume.
- 17 Copin-Montegut, C., and Copin-Montegut, G.: The chemistry of particulate matter from the  
18 south Indian and Antarctic oceans, *Deep Sea Research*, 25, 911-931, 10.1016/0146-  
19 6291(78)90633-1, 1978.
- 20 Cullen, J. J.: The Deep Chlorophyll Maximum: Comparing Vertical Profiles of Chlorophyll a,  
21 *Canadian Journal of Fisheries and Aquatic Sciences*, 39, 791-803, 10.1139/f82-108, 1982.
- 22 d'Ovidio, F., Zhou, M., Park, Y. H., Nencioli, F., Resplandy, L., Doglioli, A., Petrenko, A.,  
23 Blain, S., and Queguiner, B.: Guiding biogeochemical campaigns with high resolution  
24 altimetry: waiting for the SWOT mission., *Proceedings of 20 Years of Progress in Radar*  
25 *Altimetry Symposium*, Venice, Italy, 2012.
- 26 de Baar, H. J. W., Van Leeuwe, M. A., Scharek, R., Goeyens, L., Bakker, K. M. J., and  
27 Fritsche, P.: Nutrient anomalies in *Fragilariopsis kerguelensis* blooms, iron deficiency and the  
28 nitrate/phosphate ratio (A. C. Redfield) of the Antarctic Ocean, *Deep Sea Research Part II:*  
29 *Topical Studies in Oceanography*, 44, 229-260, 10.1016/S0967-0645(96)00102-6, 1997.
- 30 de Baar, H. J. W., Boyd, P., Coale, K., Landry, M., Tsuda, A., Assmy, P., Bakker, D. C.,  
31 Bozec, Y., Barber, R. T., Brzezinski, M., Buesseler, K., Boyé, M., Croot, P., Gervais, F.,  
32 Gorbunov, M., Harrison, P., Hiscock, W., Laan, P., Lancelot, C., Law, C., Levasseur, M.,  
33 Marchetti, A., Millero, F., Nishioka, J., Nojiri, Y., van Oijen, T., Riebesell, U., Rijkenberg,  
34 M., Saito, H., Takeda, S., Timmermans, K., Veldhuis, M., Waite, A., and Wong, C.-S.:  
35 Synthesis of iron fertilization experiments: From the Iron Age in the Age of Enlightenment,  
36 *Journal of Geophysical Research*, 110, C09S16, 10.1029/2004JC002601, 2005.
- 37 Dugdale, R. C., Wilkerson, F. P., and Minas, H. J.: The role of a silicate pump in driving new  
38 production, *Deep-Sea Res. I*, 42, 697-719, 10.1016/0967-0637(95)00015-X, 1995.

- 1 Ediger, D., Raine, R., Weeks, A. R., Robinson, I. S., and Sagan, S.: Pigment signatures reveal  
2 temporal and regional differences in taxonomic phytoplankton composition off the west coast  
3 of Ireland, *Journal of Plankton Research*, 23, 893-902, 10.1093/plankt/23.8.893, 2001.
- 4 Falkowski, P. G., Laws, E. A., Barber, R. T., and Murray, J. W.: Phytoplankton and Their  
5 Role in Primary, New, and Export Production, in: *Ocean Biogeochemistry*, edited by:  
6 Fasham, M. R., *Global Change - The IGBP Series*, Springer Berlin Heidelberg, 99-121, 2003.
- 7 Firme, G. F., Rue, E. L., Weeks, D. A., Bruland, K. W., and Hutchins, D. A.: Spatial and  
8 temporal variability in phytoplankton iron limitation along the California coast and  
9 consequences for Si, N, and C biogeochemistry, *Global Biogeochemical Cycles*, 17, 1016,  
10 10.1029/2001gb001824, 2003.
- 11 Franck, V. M., Brzezinski, M. A., Coale, K. H., and Nelson, D. M.: Iron and silicic acid  
12 concentrations regulate Si uptake north and south of the Polar Frontal Zone in the Pacific  
13 Sector of the Southern Ocean, *Deep Sea Research Part II: Topical Studies in Oceanography*,  
14 47, 3315-3338, 10.1016/S0967-0645(00)00070-9, 2000.
- 15 Froneman, P. W., Pakhomov, E. A., and Balarin, M. G.: Size-fractionated phytoplankton  
16 biomass, production and biogenic carbon flux in the eastern Atlantic sector of the Southern  
17 Ocean in late austral summer 1997-1998, *Deep Sea Research Part II: Topical Studies in*  
18 *Oceanography*, 51, 2715-2729, 10.1016/j.dsr2.2002.09.001, 2004.
- 19 Gall, M. P., Boyd, P. W., Hall, J., Safi, K. A., and Chang, H.: Phytoplankton processes. Part  
20 1: Community structure during the Southern Ocean Iron RElease Experiment (SOIREE),  
21 *Deep Sea Research Part II: Topical Studies in Oceanography*, 48, 2551-2570, 10.1016/S0967-  
22 0645(01)00008-X, 2001.
- 23 Gautier, I.: *Les basaltes des îles Kerguelen (Terres Australes et Antarctiques Françaises)*.  
24 Thèse de Doctorat, Université Paris VI, France, 383 pp., 1987.
- 25 Geider, R., and La Roche, J.: Redfield revisited: variability of C:N:P in marine microalgae  
26 and its biochemical basis, *European Journal of Phycology*, 37, 1-17,  
27 10.1017/s0967026201003456, 2002.
- 28 Goffart, A., Catalano, G., and Hecq, J. H.: Factors controlling the distribution of diatoms and  
29 *Phaeocystis* in the Ross Sea, *Journal of Marine Systems*, 27, 161-175, 10.1016/S0924-  
30 7963(00)00065-8, 2000.
- 31 Hare, C. E., DiTullio, G. R., Trick, C. G., Bruland, S. W. W., Rue, E. L., and Hutchins, D.  
32 A.: Phytoplankton community structure changes following simulated upwelled iron inputs in  
33 the Peru upwelling region, *Aquatic Microbial Ecology*, 38, 269-282, 10.3354/ame038269,  
34 2005.
- 35 Hare, C. E., DiTullio, G. R., Riseman, S. F., Crossley, A. C., Popels, L. C., Sedwick, P. N.,  
36 and Hutchins, D. A.: Effects of changing continuous iron input rates on a Southern Ocean  
37 algal assemblage, *Deep Sea Research Part I: Oceanographic Research Papers*, 54, 732-746,  
38 10.1016/j.dsr.2007.02.001, 2007.

- 1 Heimburger, A., Losno, R., Triquet, S., Dulac, F., and Mahowald, N.: Direct measurements of  
2 atmospheric iron, cobalt, and aluminum-derived dust deposition at Kerguelen Islands, *Global*  
3 *Biogeochemical Cycles*, 26, GB4016, 10.1029/2012gb004301, 2012.
- 4 Henjes, J., Assmy, P., Klaas, C., Verity, P., and Smetacek, V.: Response of microzooplankton  
5 (protists and small copepods) to an iron-induced phytoplankton bloom in the Southern Ocean  
6 (EisenEx), *Deep Sea Research Part I: Oceanographic Research Papers*, 54, 363-384,  
7 10.1016/j.dsr.2006.12.004, 2007.
- 8 Hoffmann, L. J., Peeken, I., Lochte, K., Assmy, P., and Veldhuis, M.: Different reactions of  
9 Southern Ocean phytoplankton size classes to iron fertilization., *Limnology and*  
10 *Oceanography*, 51, 1217-1229, 10.4319/lo.2006.51.3.1217, 2006.
- 11 Hoffmann, L. J., Peeken, I., and Lochte, K.: Effects of iron on the elemental stoichiometry  
12 during EIFEX and in the diatoms *Fragilariopsis kerguelensis* and *Chaetoceros dichaeta*,  
13 *Biogeosciences*, 4, 569-579, 10.5194/bg-4-569-2007, 2007.
- 14 Howard, A. G., Coxhead, A. J., Potter, I. A., and Watt, A. P.: Determination of dissolved  
15 aluminium by the micelle-enhanced fluorescence of its lumogallion complex, *Analyst*, 111,  
16 1379-1382, 10.1039/an9861101379, 1986.
- 17 Hutchins, D. A., and Bruland, K. W.: Iron-limited diatom growth and Si:N uptake ratios in a  
18 coastal upwelling regime, *Nature*, 393, 561-564, 10.1038/31203, 1998.
- 19 Hydes, D. J., and Liss, P. S.: Fluorimetric method for the determination of low concentrations  
20 of dissolved aluminium in natural waters, *Analyst*, 101, 922-931, 10.1039/an9760100922,  
21 1976.
- 22 Jacquet, S. H. M., Dehairs, F., Cavagna, A.-J., Planchon, F., Monin, L., and André, L.: Early  
23 season mesopelagic carbon remineralization and transfer efficiency in the naturally iron-  
24 fertilized Kerguelen area, *Biogeosciences KEOPS 2 special issue*, this volume.
- 25 Johnsen, G., and Sakshaug, E.: Bio-optical characteristics and photoadaptive responses in the  
26 toxic and bloom-forming dinoflagellates *Gyrodinium aureolum*, *Gymnodinium galatheanum*,  
27 and two strains of *Prorocentrum minimum*, *Journal of Phycology*, 29, 627-642,  
28 10.1111/j.0022-3646.1993.00627.x, 1993.
- 29 Jouandet, M. P., Blain, S., Metzl, N., Brunet, C., Trull, T. W., and Obernosterer, I.: A  
30 seasonal carbon budget for a naturally iron-fertilized bloom over the Kerguelen Plateau in the  
31 Southern Ocean, *Deep Sea Research Part II: Topical Studies in Oceanography*, 55, 856-867,  
32 10.1016/j.dsr2.2007.12.037, 2008.
- 33 Klausmeier, C. A., Litchman, E., and Levin, S. A.: Phytoplankton growth and stoichiometry  
34 under multiple nutrient limitation, *Limnology & Oceanography*, 49, 1463-1470,  
35 10.4319/lo.2004.49.4\_part\_2.1463, 2004.
- 36 Kopczyńska, E. E., Fiala, M., and Jeandel, C.: Annual and interannual variability in  
37 phytoplankton at a permanent station off Kerguelen Islands, *Southern Ocean, Polar Biology*,  
38 20, 342-351, 10.1007/s003000050312, 1998.

- 1 Lance, V. P., Hiscock, M. R., Hilting, A. K., Stuebe, D. A., Bidigare, R. R., Smith Jr, W. O.,  
2 and Barber, R. T.: Primary productivity, differential size fraction and pigment composition  
3 responses in two Southern Ocean in situ iron enrichments, *Deep Sea Research Part I:*  
4 *Oceanographic Research Papers*, 54, 747-773, 10.1016/j.dsr.2007.02.008, 2007.
- 5 Lancelot, C., Hannon, E., Becquevort, S., Veth, C., and de Baar, H. J. W.: Modeling  
6 phytoplankton blooms and carbon export production in the Southern Ocean: dominant  
7 controls by light and iron in the Atlantic sector in Austral spring 1992, *Deep Sea Research*  
8 *Part I: Oceanographic Research Papers*, 47, 1621-1662, 10.1016/S0967-0637(00)00005-4,  
9 2000.
- 10 Laurenceau, E. C., Trull, T. W., Davis, D. M., Bray, S. G., Doran, J., Planchon, F., Carlotti,  
11 F., Jouandet, M.-P., Cavagna, A.-J., Waite, A. M., and Blain, S.: Importance of ecosystem  
12 structure to carbon export: insights from free-drifting sediment trap deployments in naturally  
13 iron-fertilised waters near the Kerguelen plateau, *Biogeosciences*, KEOPS2 special issue, this  
14 volume.
- 15 Leblanc, K., Quéguiner, B., Fiala, M., Blain, S., Morvan, J., and Corvaisier, R.: Particulate  
16 biogenic silica and carbon production rates and particulate matter distribution in the Indian  
17 sector of the Subantarctic Ocean, *Deep Sea Research Part II: Topical Studies in*  
18 *Oceanography*, 49, 3189-3206, 10.1016/S0967-0645(02)00078-4, 2002.
- 19 Legendre, L., and Le Fèvre, J.: Hydrodynamical singularities as controls of recycled versus  
20 export production in oceans in: *Geological Journal*, 63 ed., edited by: Berger, W. H.,  
21 Smetacek, V. S., and Wefer, G., *Productivity of the oceans: Present and past*, Wiley, 49-63,  
22 1989.
- 23 Lévy, M., Klein, P., and Treguier, A.-M.: Impact of sub-mesoscale physics on production and  
24 subduction of phytoplankton in an oligotrophic regime, *Journal of Marine Research*, 59 535-  
25 565, 2001.
- 26 Margalef, R.: *Ecological Correlations and the Relationship Between Primary Productivity and*  
27 *Community Structure*, in: *Memorie dell'Istituto Italiano di Idrobiologia*, 355-364, 1965.
- 28 Marra, J. F., Lance, V. P., Vaillancourt, R. D., and Hargreaves, B. R.: Resolving the ocean's  
29 euphotic zone, *Deep Sea Research Part I: Oceanographic Research Papers*, 83, 45-50,  
30 10.1016/j.dsr.2013.09.005, 2014.
- 31 Martin, J. H.: Glacial-interglacial CO<sub>2</sub> change: The Iron Hypothesis, *Paleoceanography*, 5, 1-  
32 13, 10.1029/PA005i001p00001, 1990.
- 33 Martin, J. H., Gordon, R. M., and Fitzwater, S. E.: The case for iron, *Journal Name:*  
34 *Limnology and Oceanography*; (United States); *Journal Volume:* 36:8, *Medium:* X; *Size:*  
35 *Pages:* 1793-1802, 1991.
- 36 Martiny, A. C., Pham, C. T. A., Primeau, F. W., Vrugt, J. A., Moore, J. K., Levin, S. A., and  
37 Lomas, M. W.: Strong latitudinal patterns in the elemental ratios of marine plankton and  
38 organic matter, *Nature Geoscience*, 6, 279-283, 10.1038/ngeo1757, 2013.

- 1 Matsumoto, K., Sarmiento, J. L., and Brzezinski, M. A.: Silicic acid leakage from the  
2 Southern Ocean: A possible explanation for glacial atmospheric pCO<sub>2</sub>, *Global*  
3 *Biogeochemical Cycles*, 16, 3, 10.1029/2001gb001442, 2002.
- 4 Moore, C. M., Hickman, A. E., Poulton, A. J., Seeyave, S., and Lucas, M. I.: Iron-light  
5 interactions during the CROZet natural iron bloom and EXport experiment (CROZEX):  
6 Taxonomic responses and elemental stoichiometry, *Deep Sea Research Part II: Topical*  
7 *Studies in Oceanography*, 54, 2066-2084, 10.1016/j.dsr2.2007.06.015, 2007.
- 8 Morris, P. J., and Charette, M. A.: A synthesis of upper ocean carbon and dissolved iron  
9 budgets for Southern Ocean natural iron fertilisation studies, *Deep Sea Research Part II:*  
10 *Topical Studies in Oceanography*, 90, 147-157, 10.1016/j.dsr2.2013.02.001, 2013.
- 11 Mosseri, J., Quéguiner, B., Armand, L., and Cornet-Barthaux, V.: Impact of iron on silicon  
12 utilization by diatoms in the Southern Ocean: A case study of Si/N cycle decoupling in a  
13 naturally iron-enriched area, *Deep Sea Research Part II: Topical Studies in Oceanography*, 55,  
14 801-819, 10.1016/j.dsr2.2007.12.003, 2008.
- 15 Nelson, D. M., Tréguer, P., Brzezinski, M. A., Leynaert, A., and Quéguiner, B.: Production  
16 and dissolution of biogenic silica in the ocean: Revised global estimates, comparison with  
17 regional data and relationship to biogenic sedimentation, *Global Biogeochemical Cycles*, 9,  
18 359-372, 10.1029/95gb01070, 1995.
- 19 Park, Y.-H., and Gamberoni, L.: Cross-frontal exchange of Antarctic Intermediate Water and  
20 Antarctic Bottom Water in the Crozet Basin, *Deep Sea Research Part II: Topical Studies in*  
21 *Oceanography*, 44, 963-986, 10.1016/S0967-0645(97)00004-0, 1997.
- 22 Park, Y.-H., Fuda, J.-L., Durand, I., and Naveira Garabato, A. C.: Internal tides and vertical  
23 mixing over the Kerguelen Plateau, *Deep Sea Research Part II: Topical Studies in*  
24 *Oceanography*, 55, 582-593, 10.1016/j.dsr2.2007.12.027, 2008a.
- 25 Park, Y.-H., Roquet, F., Durand, I., and Fuda, J.-L.: Large-scale circulation over and around  
26 the Northern Kerguelen Plateau, *Deep Sea Research Part II: Topical Studies in*  
27 *Oceanography*, 55, 566-581, 10.1016/j.dsr2.2007.12.030, 2008b.
- 28 Park, Y.-H., Durand, I., Kestenare, E., Rougier, G., Zhou, M., d'Ovidio, F., and Lee, J.-H.:  
29 Polar Front around Kerguelen: An up-to-date determination and associated circulation of  
30 subsurface waters, *Biogeosciences KEOPS2 special issue*, this volume.
- 31 Peeken, I.: Photosynthetic pigment fingerprints as indicators of phytoplankton biomass and  
32 development in different water masses of the Southern Ocean during austral spring, *Deep Sea*  
33 *Research Part II: Topical Studies in Oceanography*, 44, 261-282, 10.1016/S0967-  
34 0645(96)00077-X, 1997.
- 35 Planchon, F., Ballas, D., Cavagna, A.-J., van der Merwe, P., Bowie, A. W., Trull, T.,  
36 Laurenceau, E. C., Davies, D. M., and Dehairs, F.: Carbon export in the naturally iron-  
37 fertilized Kerguelen area of the Southern Ocean using <sup>234</sup>Th based approach, *Biogeosciences*  
38 *KEOPS 2 special issue*, this volume.

- 1 Pollard, R. T., Salter, I., Sanders, R. J., Lucas, M. I., Moore, C. M., Mills, R. A., Statham, P.  
2 J., Allen, J. T., Baker, A. R., Bakker, D. C. E., Charette, M. A., Fielding, S., Fones, G. R.,  
3 French, M., Hickman, A. E., Holland, R. J., Hughes, J. A., Jickells, T. D., Lampitt, R. S.,  
4 Morris, P. J., Nedelec, F. H., Nielsdottir, M., Planquette, H., Popova, E. E., Poulton, A. J.,  
5 Read, J. F., Seeyave, S., Smith, T., Stinchcombe, M., Taylor, S., Thomalla, S., Venables, H.  
6 J., Williamson, R., and Zubkov, M. V.: Southern Ocean deep-water carbon export enhanced  
7 by natural iron fertilization, *Nature*, 457, 577-580, 10.1038/nature07716, 2009.
- 8 Price, N. M.: The elemental stoichiometry and composition of an iron-limited diatom,  
9 *Limnology and Oceanography*, 50, 1159-1171, 10.4319/lo.2005.50.4.1159, 2005.
- 10 Pujo-Pay, M., and Raimbault, P.: Improvement of the wet-oxidation procedure for  
11 simultaneous determination of particulate organic nitrogen and phosphorus collected on  
12 filters, *Marine Ecology Progress Series*, 105, 203-207, 1994.
- 13 Quéguiner, B., Tréguer, P., Peeken, I., and Scharek, R.: Biogeochemical dynamics and the  
14 silicon cycle in the Atlantic sector of the Southern Ocean during austral spring 1992, *Deep  
15 Sea Research Part II: Topical Studies in Oceanography*, 44, 69-89, 10.1016/S0967-  
16 0645(96)00066-5, 1997.
- 17 Quéguiner, B.: Biogenic silica production in the Australian sector of the Subantarctic Zone of  
18 the Southern Ocean in late summer 1998, *Journal of Geophysical Research: Oceans*, 106,  
19 31627-31636, 10.1029/2000jc000249, 2001.
- 20 Quéguiner, B., and Brzezinski, M. A.: Biogenic silica production rates and particulate organic  
21 matter distribution in the Atlantic sector of the Southern Ocean during austral spring 1992,  
22 *Deep Sea Research Part II: Topical Studies in Oceanography*, 49, 1765-1786, 10.1016/S0967-  
23 0645(02)00011-5, 2002.
- 24 Quéguiner, B.: Iron fertilization and the structure of planktonic communities in high nutrient  
25 regions of the Southern Ocean, *Deep Sea Research Part II: Topical Studies in Oceanography*,  
26 90, 43-54, 10.1016/j.dsr2.2012.07.024, 2013.
- 27 Quéroué, F., Sarthou, G., Chever, F., Van der Merwe, P., Lannuzel, D., Townsend, A.,  
28 Bucciarelli, E., Planquette, H., Cheize, M., Blain, S., d'Ovidio, F., and Bowie, A.: A new  
29 study of natural Fe fertilization processes in the vicinity of the Kerguelen Islands (KEOPS2  
30 experiment), *Biogeosciences KEOPS 2 special issue*, this volume.
- 31 Ragueneau, O., Savoye, N., Del Amo, Y., Cotten, J., Tardiveau, B., and Leynaert, A.: A new  
32 method for the measurement of biogenic silica in suspended matter of coastal waters: using  
33 Si:Al ratios to correct for the mineral interference, *Continental Shelf Research*, 25, 697-710,  
34 10.1016/j.csr.2004.09.017, 2005.
- 35 Ras, J., Claustre, H., and Uitz, J.: Spatial variability of phytoplankton pigment distributions in  
36 the Subtropical South Pacific Ocean: comparison between in situ and predicted data,  
37 *Biogeosciences*, 5, 353-369, 10.5194/bg-5-353-2008, 2008.
- 38 Read, J. F., Pollard, R. T., and Allen, J. T.: Sub-mesoscale structure and the development of  
39 an eddy in the Subantarctic Front north of the Crozet Islands, *Deep Sea Research Part II:  
40 Topical Studies in Oceanography*, 54, 1930-1948, 10.1016/j.dsr2.2007.06.013, 2007.



- 1 Redfield, A. C., Ketchum, B. H., and Richards, F. A.: The influence of organisms on the  
2 composition of sea water, in: *The Sea*, edited by: Hill, M. N., Wiley-Interscience, New York,  
3 2677, 1963.
- 4 Sarmiento, J. L., Gruber, N., Brzezinski, M. A., and Dunne, J. P.: High-latitude controls of  
5 thermocline nutrients and low latitude biological productivity, *Nature*, 427, 56-60,  
6 10.1038/nature02127, 2004.
- 7 Sarthou, G., Vincent, D., Christaki, U., Obernosterer, I., Timmermans, K. R., and Brussaard,  
8 C. P. D.: The fate of biogenic iron during a phytoplankton bloom induced by natural  
9 fertilisation: Impact of copepod grazing, *Deep Sea Research Part II: Topical Studies in*  
10 *Oceanography*, 55, 734-751, 10.1016/j.dsr2.2007.12.033, 2008.
- 11 Sarthou, G., Chever, F., Qu  rou  , F., Bowie, A. R., van der Merwe, P., Cheize, M., Sirois, M.,  
12 and Bucciarelli, E.: Fe-Cu impact in incubation experiments of natural plankton communities  
13 and Fe- and Cu-binding ligand production at the vicinity of the Kerguelen Islands, *Southern*  
14 *Ocean, Biogeosciences KEOPS 2 special issue*, this volume.
- 15 Schl  ter, M., and Rickert, D.: Effect of pH on the measurement of biogenic silica, *Marine*  
16 *Chemistry*, 63, 81-92, 10.1016/S0304-4203(98)00052-8, 1998.
- 17 Smetacek, V., Klaas, C., Strass, V. H., Assmy, P., Montresor, M., Cisewski, B., Savoye, N.,  
18 Webb, A., d'Ovidio, F., Arrieta, J. M., Bathmann, U., Bellerby, R., Berg, G. M., Croot, P.,  
19 Gonzalez, S., Henjes, J., Herndl, G. J., Hoffmann, L. J., Leach, H., Losch, M., Mills, M. M.,  
20 Neill, C., Peeken, I., Rottgers, R., Sachs, O., Sauter, E., Schmidt, M. M., Schwarz, J.,  
21 Terbruggen, A., and Wolf-Gladrow, D.: Deep carbon export from a Southern Ocean iron-  
22 fertilized diatom bloom, *Nature*, 487, 313-319, dx.doi.org/10.1038/nature11229, 2012.
- 23 Strickland, J. D. H., and Parsons, T. R.: *A practical handbook of seawater analysis*, Second  
24 ed., Fisheries Research Board of Canada, Ottawa, Canada, 310 pp., 207-226, 1972.
- 25 Sunda, W. G., and Huntsman, S. A.: Interrelated influence of iron, light and cell size on  
26 marine phytoplankton growth, *Nature*, 390, 389-392, 10.1038/37093, 1997.
- 27 Takeda, S.: Influence of iron availability on nutrient consumption ratio of diatoms in oceanic  
28 waters, *Nature*, 393, 774-777, 10.1038/31674, 1998.
- 29 Tarling, G. A., Ward, P., Atkinson, A., Collins, M. A., and Murphy, E. J.: DISCOVERY  
30 2010: Spatial and temporal variability in a dynamic polar ecosystem, *Deep Sea Research Part*  
31 *II: Topical Studies in Oceanography*, 59-60, 1-13, 10.1016/j.dsr2.2011.10.001, 2012.
- 32 Tester, P. A., Geesey, M. E., Guo, C., Paerl, H. W., and Millie, D.: Evaluating phytoplankton  
33 dynamics in the Newport River Estuary (North Carolina, USA) by HPLC-derived pigment  
34 profiles, *Marine Ecology Progress Series*, 124, 237-245, 10.3354/meps124237, 1995.
- 35 Timmermans, K. R., Gerringa, L. J., Baar, H. J. d., van der Wagt, B., Veldhuis, M. J., Jong, J.  
36 T. d., Croot, P. L., and Boye, M.: Growth rates and small Southern Ocean diatoms in relation  
37 to availability of iron in natural seawater, *Limnology and Oceanography*, 46, 260-266,  
38 10.4319/lo.2001.46.2.0260, 2001.

- 1 Timmermans, K. R., Veldhuis, M. J. W., Laan, P., and Brussaard, C. P. D.: Probing natural  
2 iron fertilization near the Kerguelen (Southern Ocean) using natural phytoplankton  
3 assemblages and diatom cultures, *Deep Sea Research Part II: Topical Studies in*  
4 *Oceanography*, 55, 693-705, 10.1016/j.dsr2.2007.12.008, 2008.
- 5 Tréguer, P., Gueneley, S., and Kamatani, A.: Biogenic silica and particulate organic matter  
6 from the Indian sector of the Southern Ocean, *Marine Chemistry*, 23, 167-180, 10.1016/0304-  
7 4203(88)90030-8, 1988.
- 8 Trull, T. W., Davies, D., and Casciotti, K.: Insights into nutrient assimilation and export in  
9 naturally iron-fertilized waters of the Southern Ocean from nitrogen, carbon and oxygen  
10 isotopes, *Deep Sea Research Part II: Topical Studies in Oceanography*, 55, 820-840,  
11 10.1016/j.dsr2.2007.12.035, 2008.
- 12 Uitz, J., Claustre, H., Morel, A., and Hooker, S. B.: Vertical distribution of phytoplankton  
13 communities in open ocean: An assessment based on surface chlorophyll, *Journal of*  
14 *Geophysical Research: Oceans*, 111, C08005, 10.1029/2005jc003207, 2006.
- 15 Uitz, J., Claustre, H., Griffiths, F. B., Ras, J., Garcia, N., and Sandroni, V.: A phytoplankton  
16 class-specific primary production model applied to the Kerguelen Islands region (Southern  
17 Ocean), *Deep Sea Research Part I: Oceanographic Research Papers*, 56, 541-560,  
18 10.1016/j.dsr.2008.11.006, 2009.
- 19 van Beek, P., Bourquin, M., Reyss, J. L., Souhaut, M., Charette, M. A., and Jeandel, C.:  
20 Radium isotopes to investigate the water mass pathways on the Kerguelen Plateau (Southern  
21 Ocean), *Deep Sea Research Part II: Topical Studies in Oceanography*, 55, 622-637,  
22 10.1016/j.dsr2.2007.12.025, 2008.
- 23 van der Merwe, P., Bowie, A., Quéroué, F., Sarthou, G., Chever, F., Trull, T., Armand, L.,  
24 Davis, D., Dehairs, F., Townsend, A. R., and Blain, S.: Sourcing the iron in the naturally  
25 fertilised bloom around the Kerguelen plateau: particulate trace metal dynamics,  
26 *Biogeosciences*, KEOPS2 special issue, this volume.
- 27 Van Heukelem, L., and Thomas, C. S.: Computer-assisted high-performance liquid  
28 chromatography method development with applications to the isolation and analysis of  
29 phytoplankton pigments, 1, Elsevier, Amsterdam, Pays-bas, 2001.
- 30 Vidussi, F., Claustre, H., Manca, B. B., Luchetta, A., and Marty, J.-C.: Phytoplankton  
31 pigment distribution in relation to upper thermocline circulation in the eastern Mediterranean  
32 Sea during winter, *Journal of Geophysical Research: Oceans*, 106, 19939-19956,  
33 10.1029/1999jc000308, 2001.
- 34 Wilks, J. V.: Diatom distribution and community composition variability on the seafloor in a  
35 naturally iron fertilised region of the Southern Ocean, Unpublished Honours Thesis,  
36 Macquarie University: North Ryde, Australia, 74 pp., 2013.
- 37 Wright, S. W., and Jeffrey, S. W.: Fucoxanthin pigment markers of marine phytoplankton  
38 analysed by HPLC and HPTLC, *Marine Ecology Progress Series*, 38, 259-266,  
39 10.3354/meps038259, 1987.

- 1 Wright, S. W., and van den Enden, R. L.: Phytoplankton community structure and stocks in  
 2 the East Antarctic marginal ice zone (BROKE survey, January-March 1996) determined by  
 3 CHEMTAX analysis of HPLC pigment signatures, Deep Sea Research Part II: Topical  
 4 Studies in Oceanography, 47, 2363-2400, 10.1016/S0967-0645(00)00029-1, 2000.
- 5 Zhou, M., Zhu, Y., Dorland, R. D., and Measures, C. I.: Dynamics of the current system in the  
 6 southern Drake Passage, Deep Sea Research Part I: Oceanographic Research Papers, 57,  
 7 1039-1048, 10.1016/j.dsr.2010.05.012, 2010.
- 8 Zhou, M., Zhu, Y., Measures, C. I., Hatta, M., Charette, M. A., Gille, S. T., Frants, M., Jiang,  
 9 M., and Greg Mitchell, B.: Winter mesoscale circulation on the shelf slope region of the  
 10 southern Drake Passage, Deep Sea Research Part II: Topical Studies in Oceanography, 90, 4-  
 11 14, 10.1016/j.dsr2.2013.03.041, 2013.
- 12 Zhou, M., Zhu, Y., d'Ovidio, F., Park, Y.-H., Durand, I., Kestenare, E., Sanial, V., van Beek,  
 13 P., Quéguiner, B., Carlotti, F., and Blain, S.: Surface currents and upwelling in Kerguelen  
 14 Plateau regions, Biogeosciences KEOPS 2 special issue, this volume.

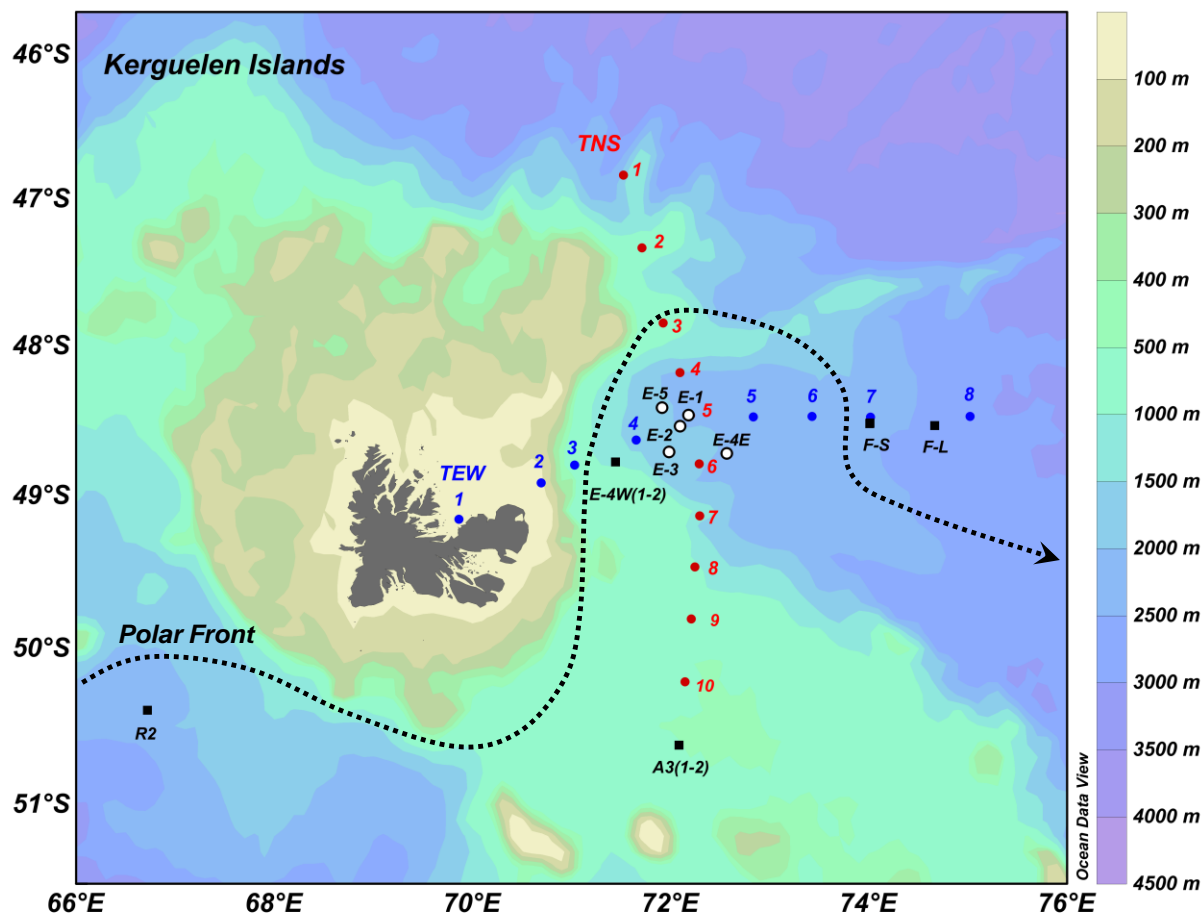
15

16 Table 1. Integrated concentrations in BSi, POC, PON and POP (in  $\text{mmol m}^{-2}$ ) over 200 m  
 17 depth (except for the coastal station TEW-2, integrated over 70 m) North and South of  
 18 the Polar Front.

19

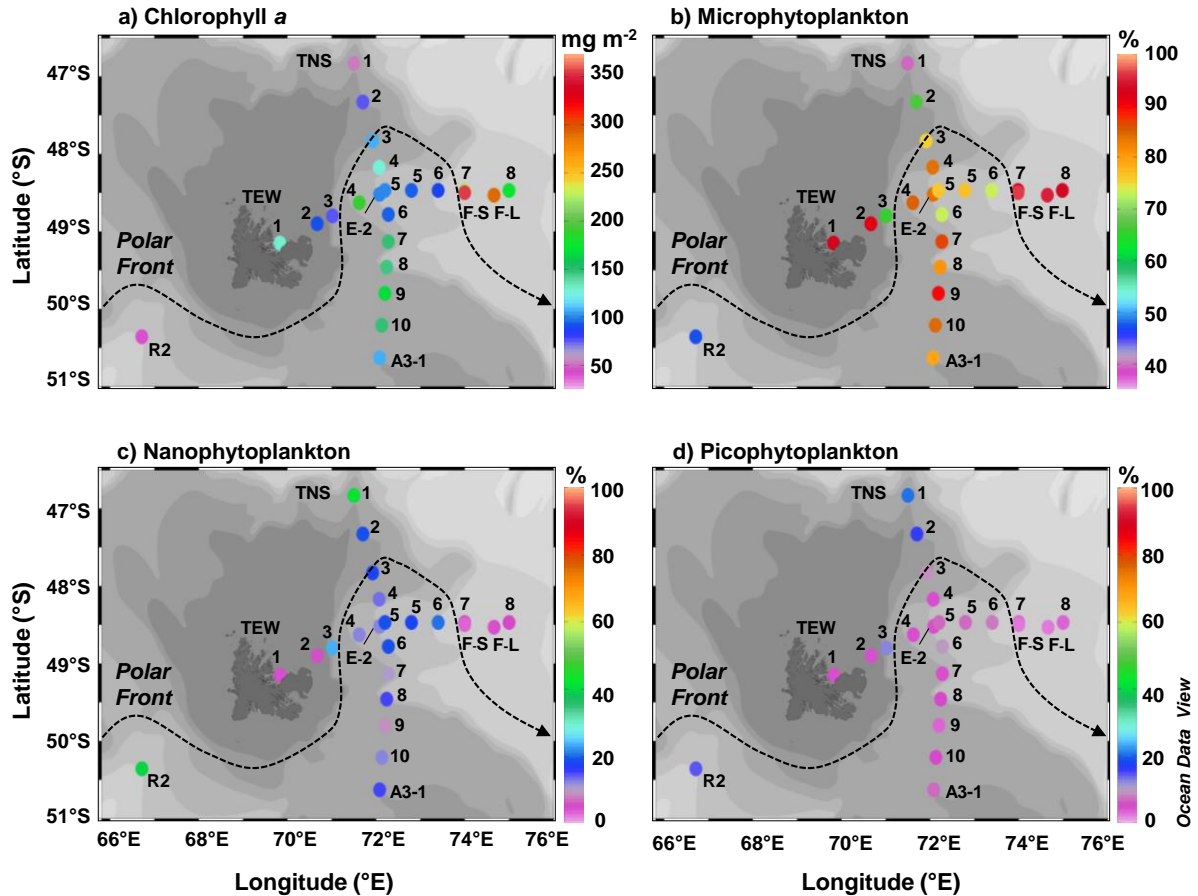
	Integrated concentrations ( $\text{mmol m}^{-2}$ )	
	North of the PF (Stations TEW-2, TEW-3, TNS-1, TNS-2)	South of the PF (Stations TEW-4 to TEW-6, TNS-3 to TNS-10, A3-1)
$\Sigma$ BSi	33.5 - 141.0	240.0 - 460.3
$\Sigma$ POC	456.9 - 629.6	562.9 - 1,164.2
$\Sigma$ PON	83.1 - 144.9	143.5 - 250.3
$\Sigma$ POP	5.7 - 10.1	8.7 - 18.9

20

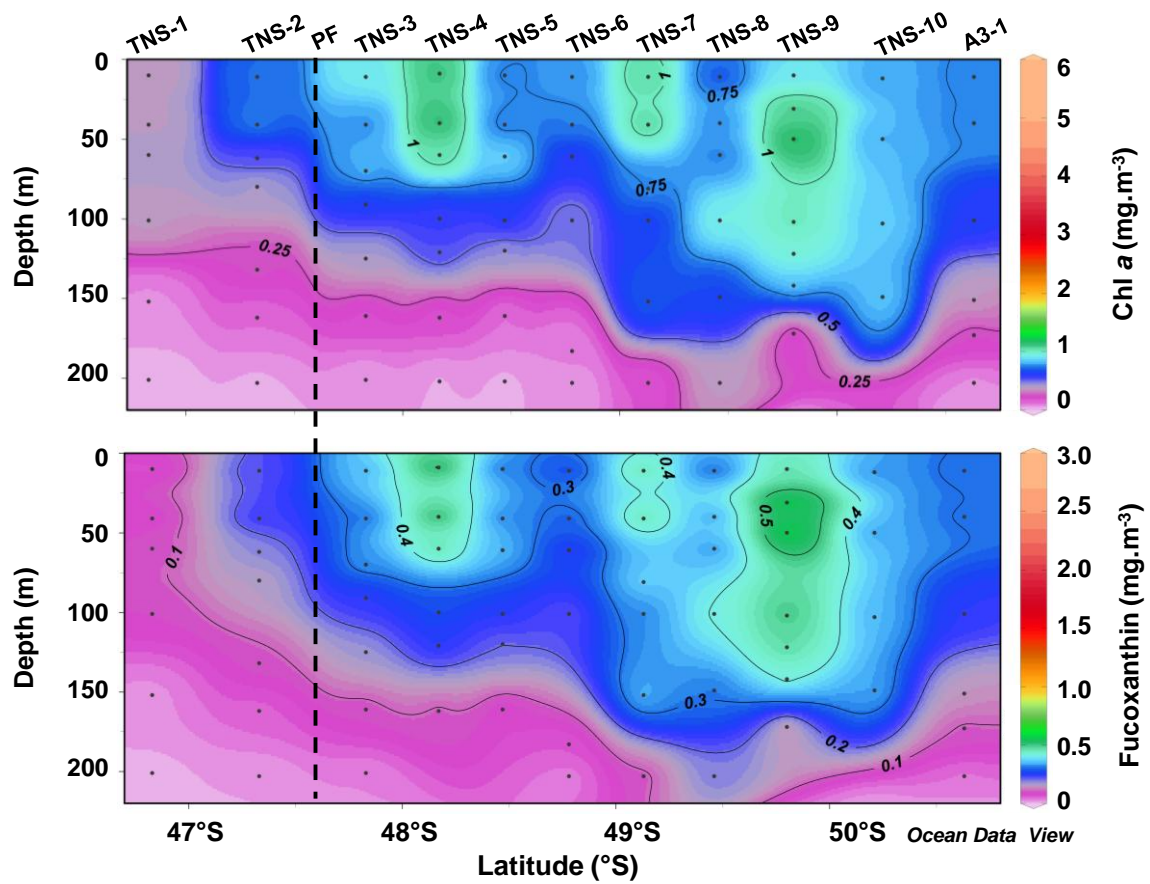


1  
 2 Figure 1. Location of the sampling stations. Transects from North to South (TNS) and from  
 3 West to the East (TEW) are indicated in red and blue respectively. The blank filled circles  
 4 correspond to a time-series of a recirculation system (E-1, E-2, E-3, E-4E and E-5). The  
 5 stations F-L and F-S are located in the eastern bloom in the Polar Front Zone. A3 and E-4W  
 6 are respectively the reference southeastern Kerguelen Plateau bloom and the reference eastern  
 7 flank of the Kerguelen Plateau. Both were visited twice (1-2). R2 is the HNLC reference  
 8 station. The dotted line represents the approximate location of the southern branch of the  
 9 Polar Front.

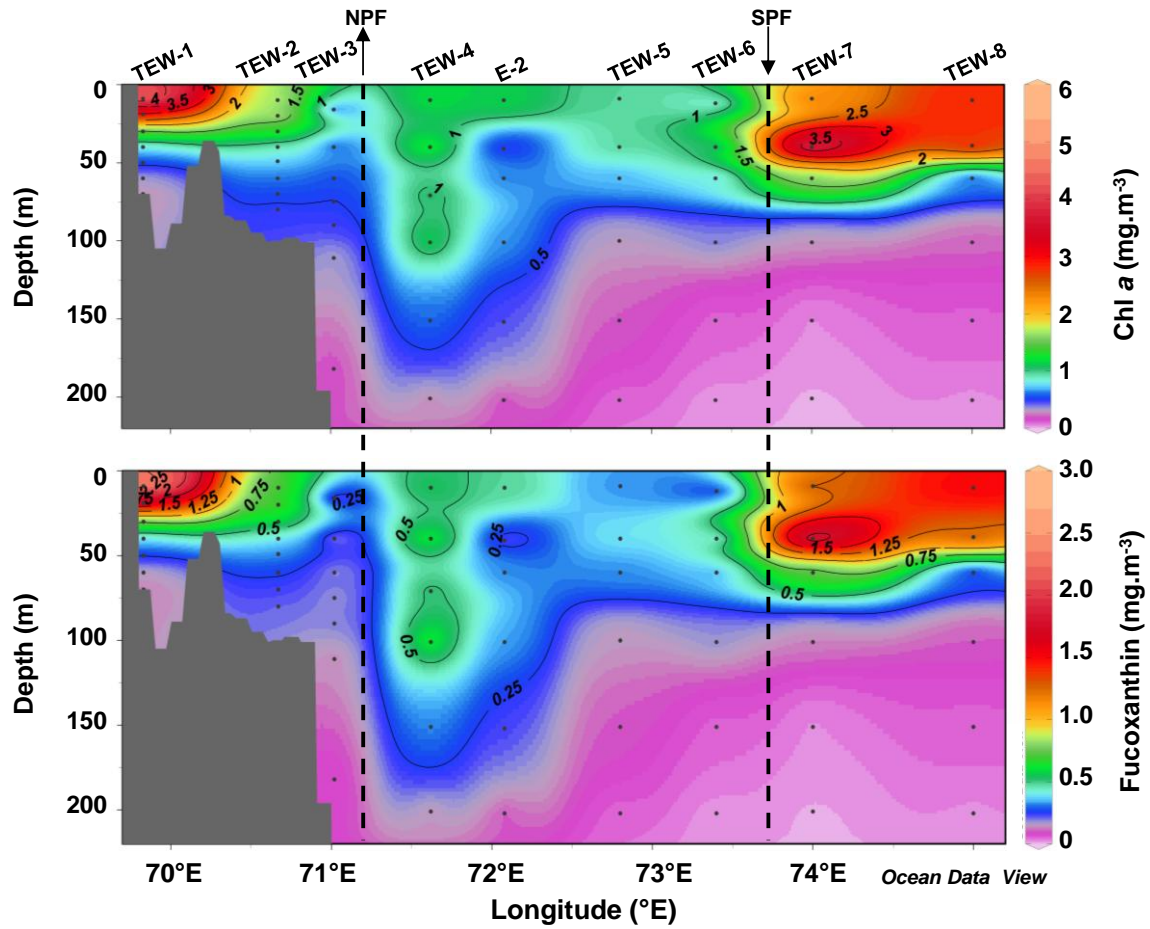
10



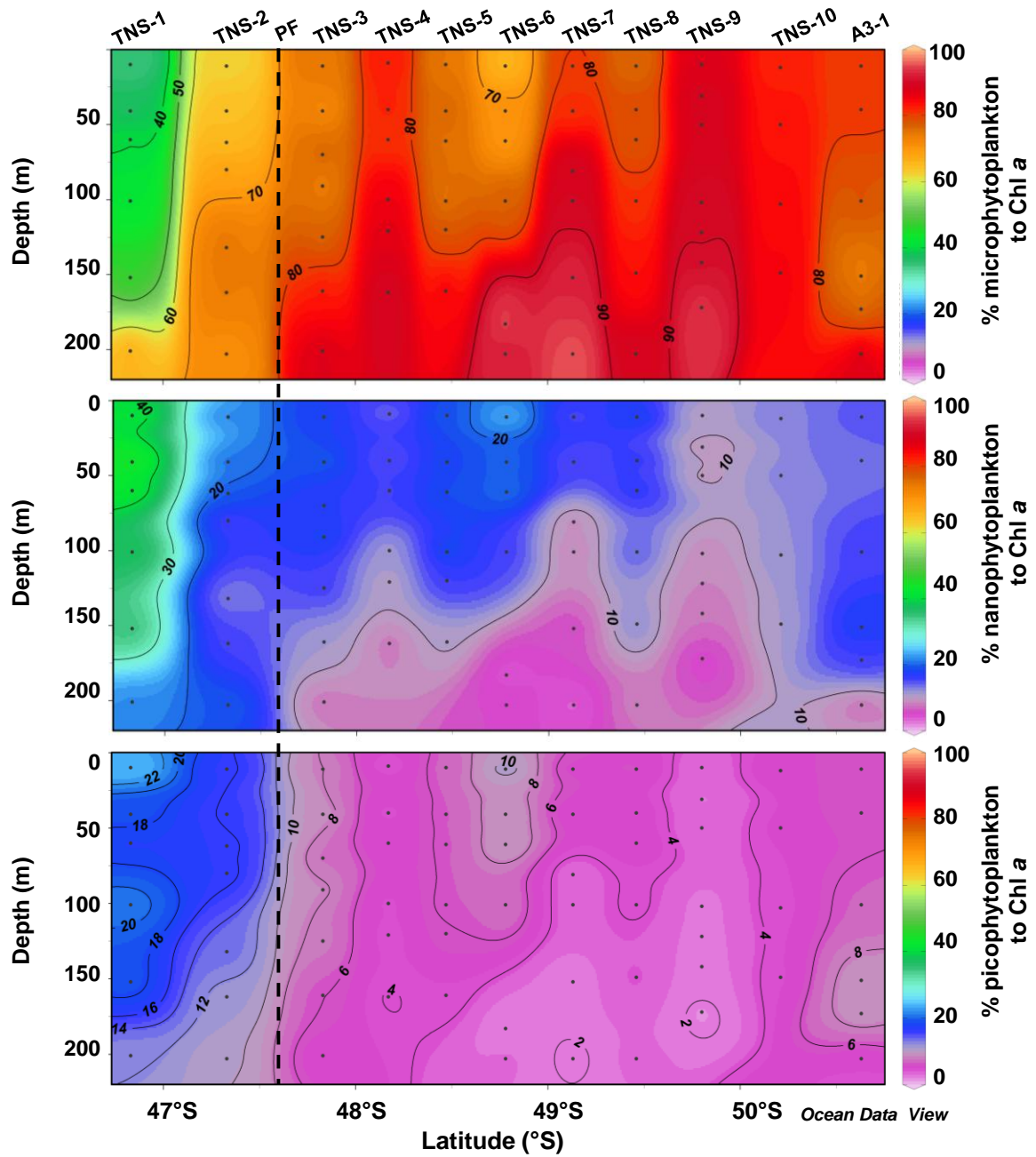
1  
 2 Figure 2. Distribution of depth-integrated total chlorophyll *a* (a) and contribution of micro-  
 3 (b), nano- (c), picophytoplankton (d) communities to total biomass. Vertical integrations were  
 4 made from the surface to 200 m except for the coastal stations TEW-1 and TEW-2 where data  
 5 were integrated down to 70 m. The TNS transect (comprising A3-1) was sampled from the  
 6 20<sup>th</sup> to the 23<sup>rd</sup> October, while the TEW transect (comprising E-2) was sampled between the  
 7 31<sup>th</sup> October and 2<sup>nd</sup> November. Station R2 was sampled between the two transects on the 25<sup>th</sup>  
 8 October, while stations F were sampled after the two transects, on the 6<sup>th</sup> November (F-L),  
 9 and the 8<sup>th</sup> November (F-S). The dashed line represents the Polar Front trajectory.  
 10



1  
 2 Figure 3. Vertical distribution of total chlorophyll *a* (Chl *a*) and fucoxanthin concentrations  
 3 along the TNS transect. The dashed line represents the approximate location of the southern  
 4 branch of the Polar Front (PF).  
 5

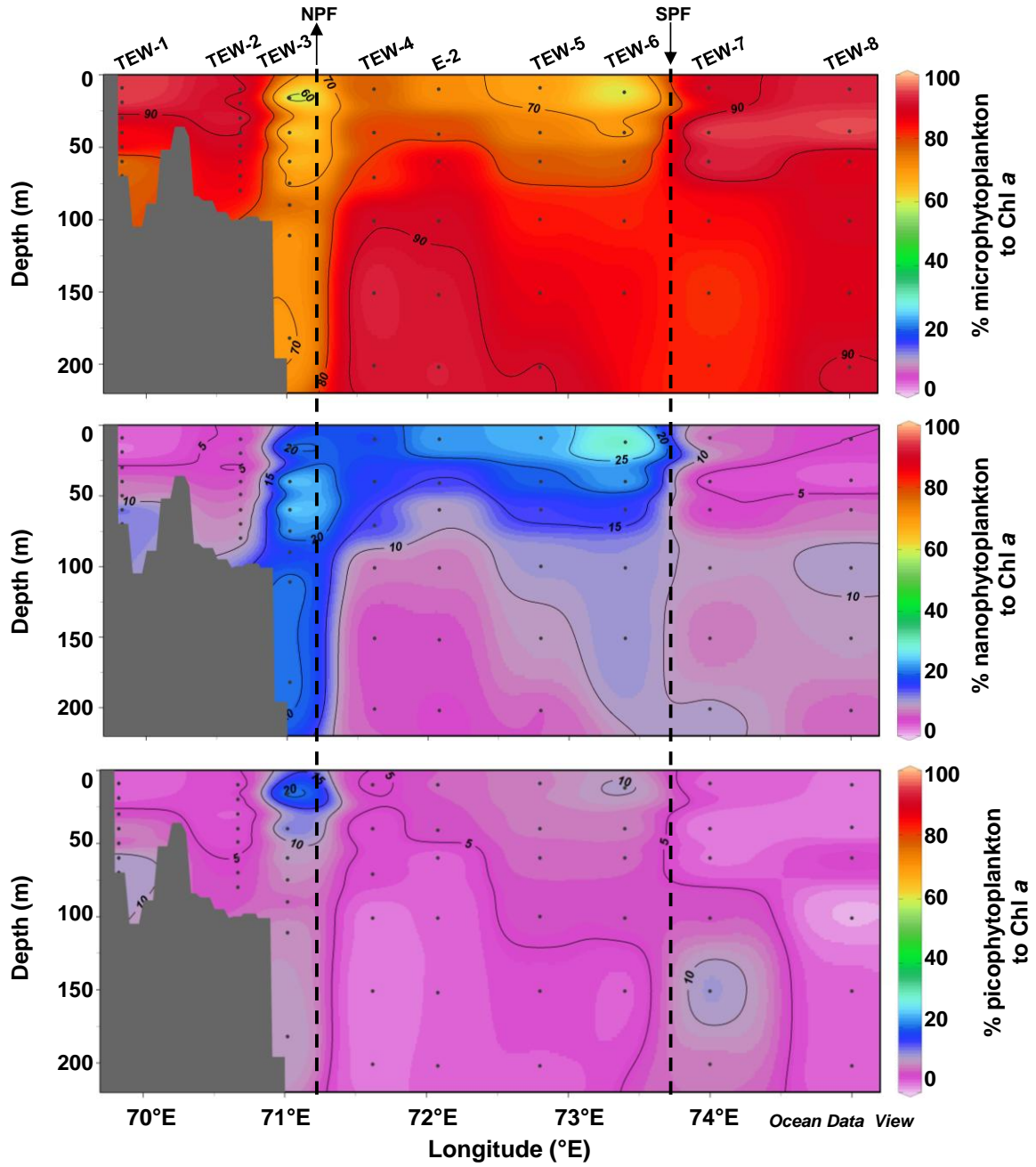


1  
 2 Figure 4. Vertical distribution of total chlorophyll *a* (Chl *a*) and fucoxanthin concentrations  
 3 along the TEW transect. The dashed lines represent the approximate location of the southern  
 4 branch of the Polar Front going to the north (NPF) and to the south (SPF).  
 5

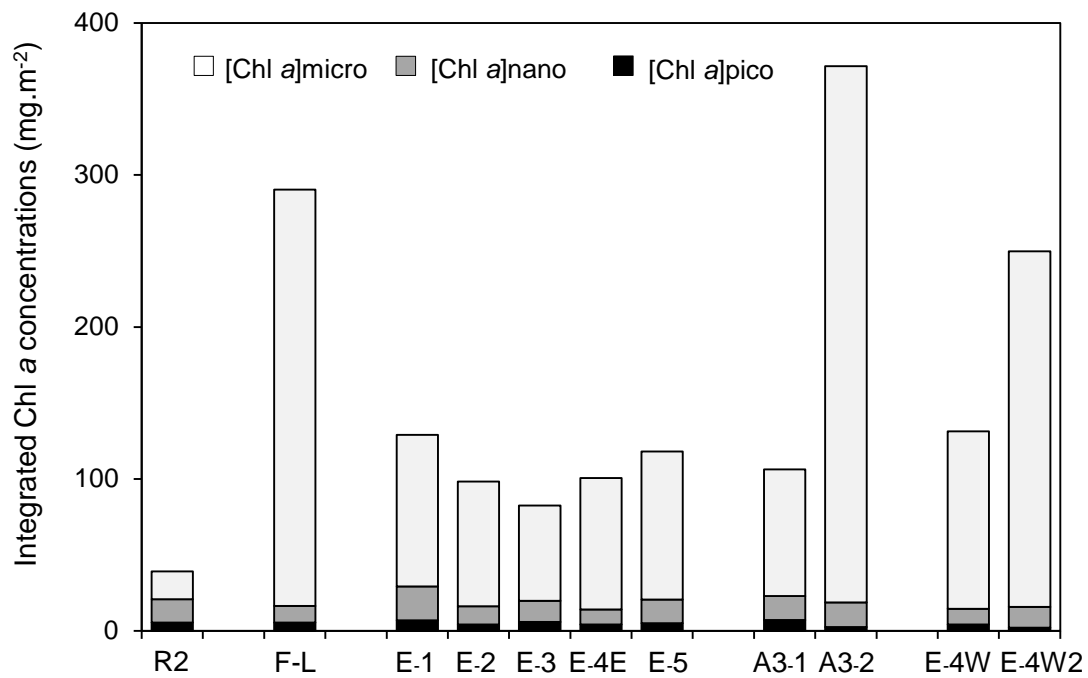


1  
 2 Figure 5. Vertical distribution of micro-, nano- and picophytoplankton community  
 3 contributions to total biomass along the TNS transect. The dashed line represents the  
 4 approximate location of the southern branch of the Polar Front (PF).  
 5





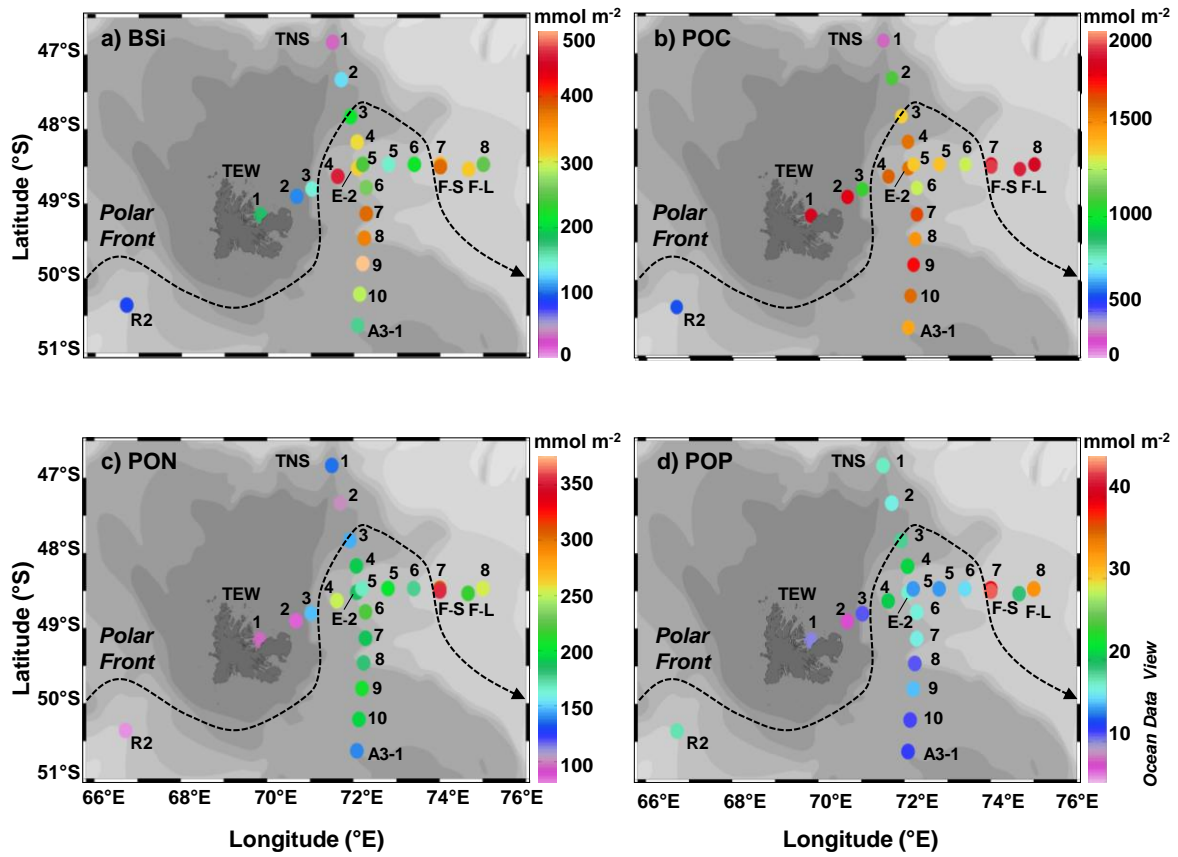
1  
 2 Figure 6. Vertical distribution of micro-, nano- and picophytoplankton community  
 3 contributions to total biomass along the TEW transect. The dashed lines represent the  
 4 approximate location of the southern branch of the Polar Front going to the North (NPF) and  
 5 to the South (SPF).  
 6



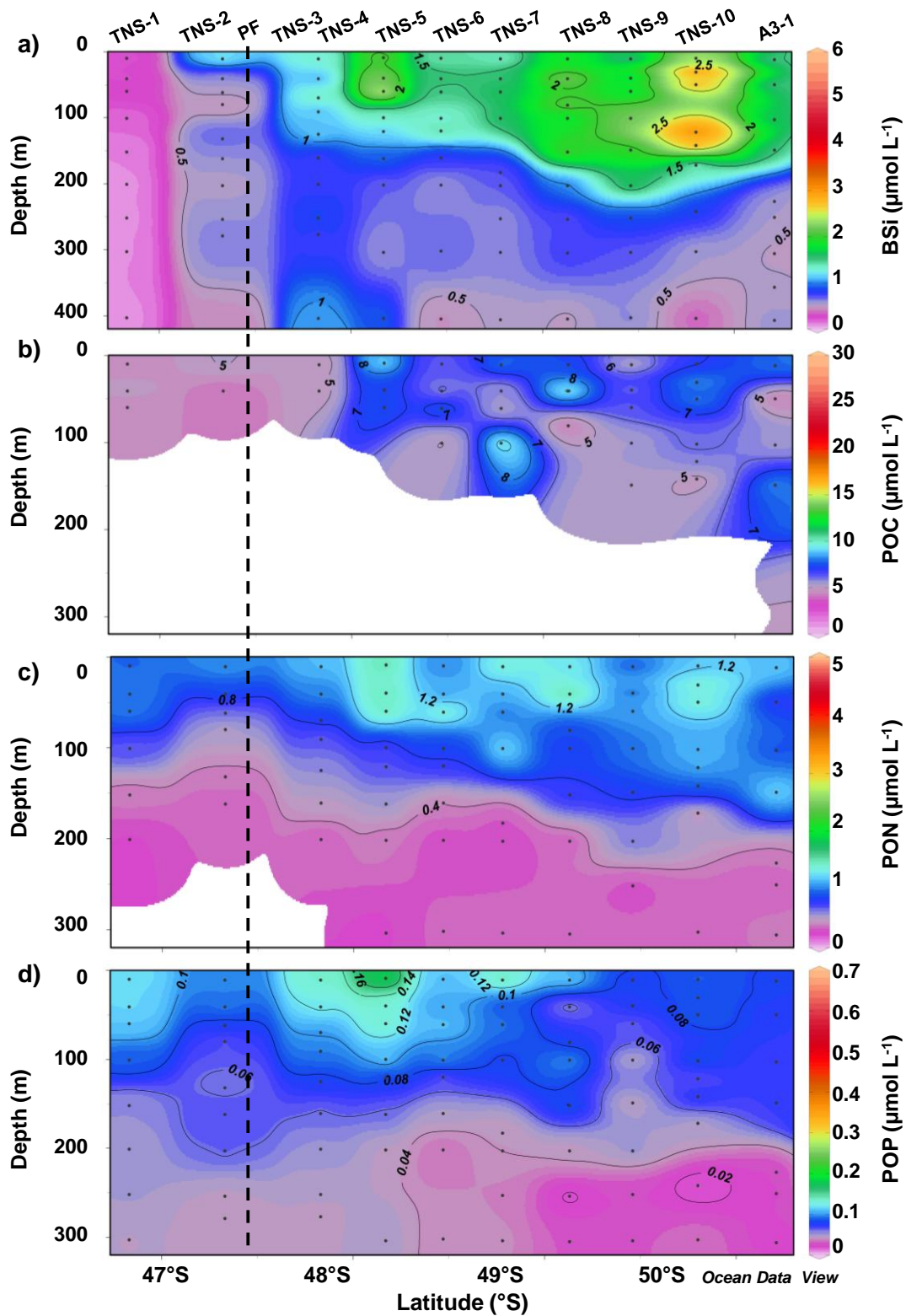
1

2 Figure 7. Temporal evolution of Chl *a* concentrations associated with micro- ([Chl *a*]micro),  
 3 nano- ([Chl *a*]nano) and picophytoplankton ([Chl *a*]pico) within 200 m at the complex system  
 4 of recirculation (five visits chronologically numerated : E-1 (10/29) , E-2 (11/01), E-3  
 5 (11/03), E-4E (11/13), E-5 (11/19)), at the plateau reference station A3 (two visits: A3-1  
 6 (10/20) and A3-2 (11/16)) and at station E-4W (two visits : E-4W (11/12) and E-4W2  
 7 (11/18)). The station F-L (integrated within 150 m) and the HNLC reference station R2 are  
 8 presented for comparison.

9

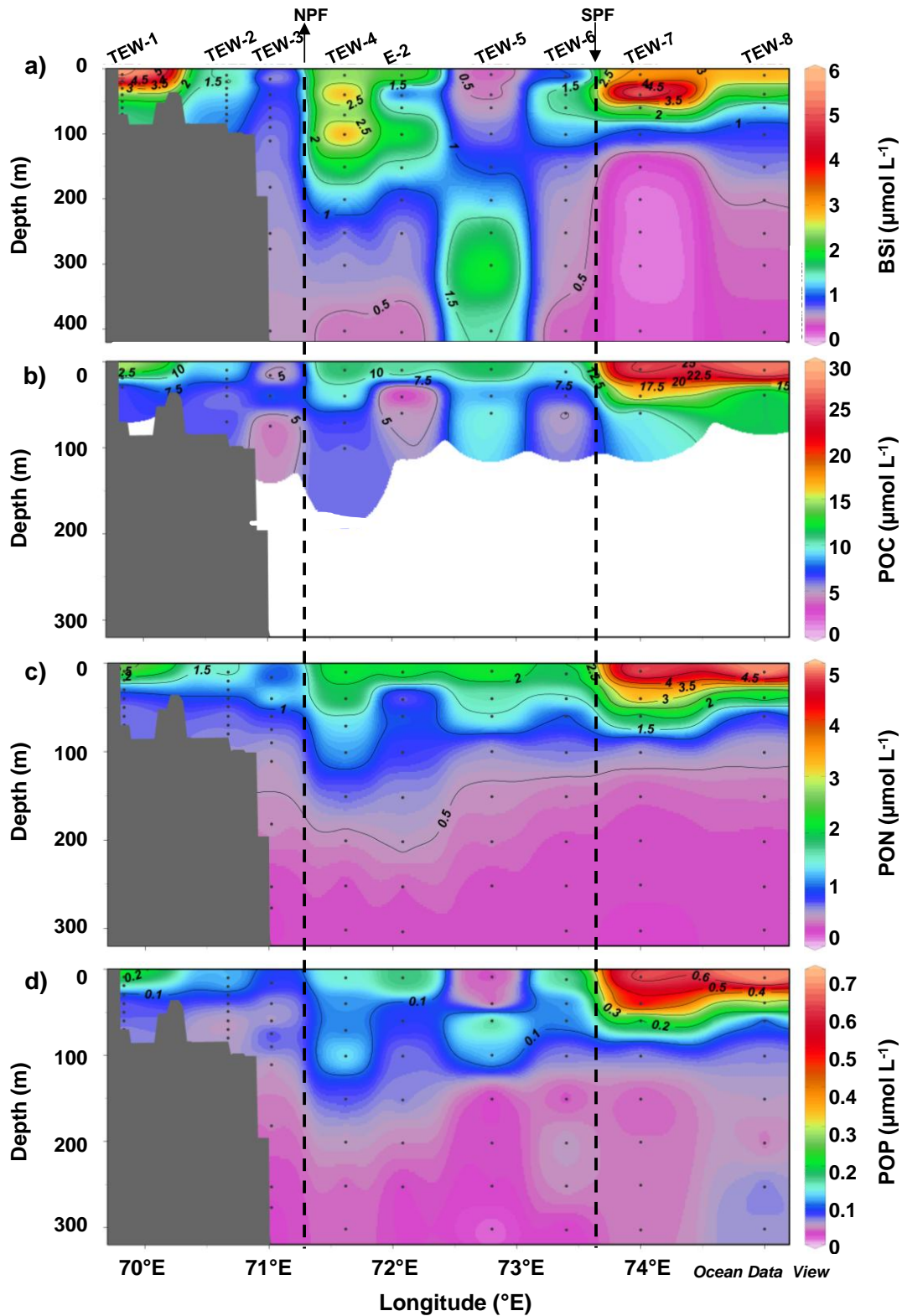


1  
 2 Figure 8. Distribution of biogenic silica (a), particulate organic carbon (b), nitrogen (c) and  
 3 phosphorus (d) (same vertical integrations and legends as Fig. 2).

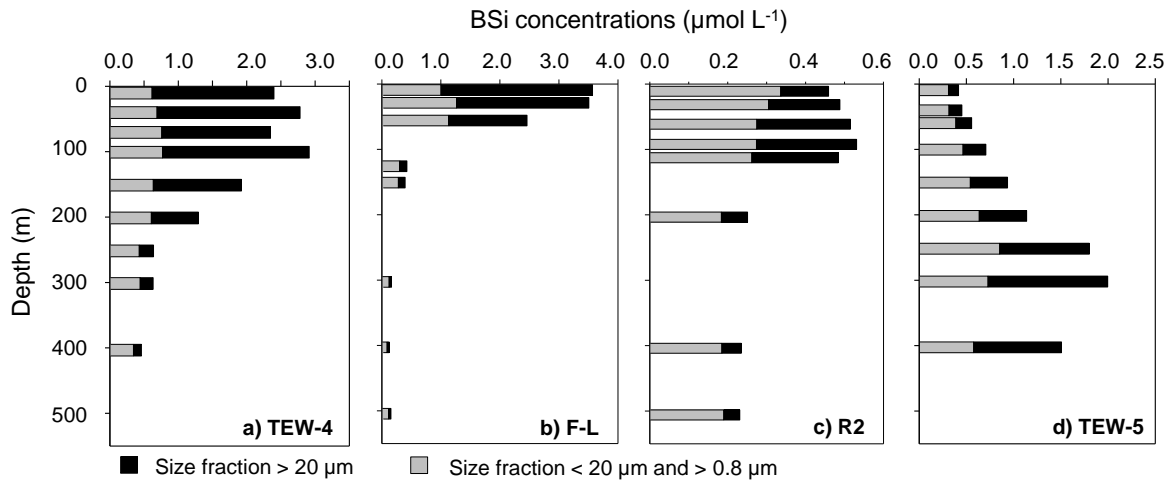


1

2 Figure 9. Vertical distributions of BSi (a), POC (b), PON (c), POP (d) concentrations along  
 3 the TNS transect. The dashed line represents the approximate location of the southern branch  
 4 of the Polar Front (PF).



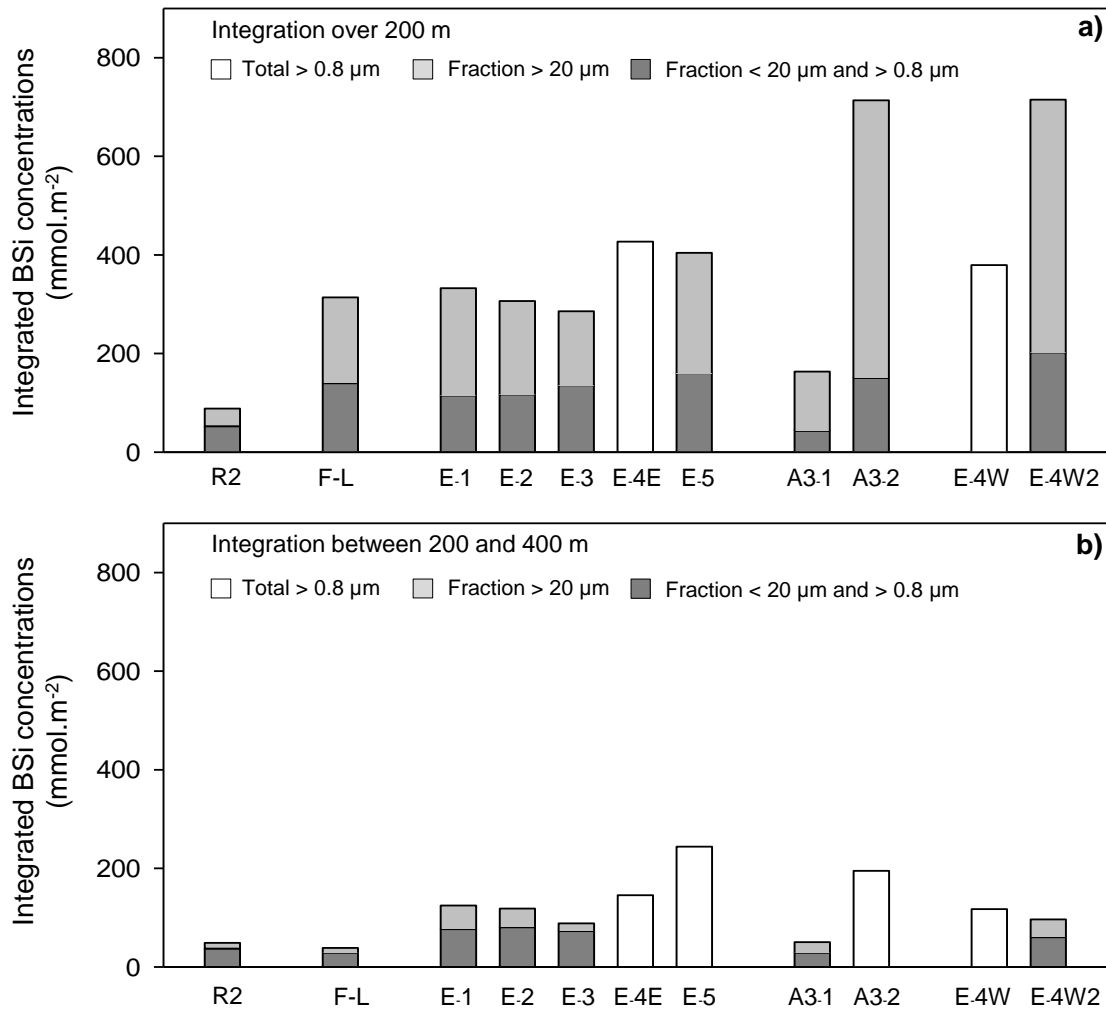
1  
 2 Figure 10. Vertical distributions of BSi (a), POC (b), PON (c), POP (d) concentrations along  
 3 the TEW transect. The dashed lines represent the approximate location of the southern branch  
 4 of the Polar Front going to the North (NPF) and to the South (SPF).



1

2 Figure 11. Vertical profiles of BSi concentrations for two size fractions (> 20 µm in black and  
 3 between 0.8 and 20 µm in grey) at TEW-4 (a), F-L (b), R2 (c) and TEW-5 (d). These four  
 4 stations were chosen to illustrate the four typical vertical profiles observed over the study  
 5 area: TEW-4 represents typical profile of the stations A3-2 and E (from E-1 to E-5), F-L  
 6 represents typical profile of stations E-4W and those located in the PFZ, R2 represents typical  
 7 profile of the low productive stations (R2, TNS-1, TNS-2, TEW-2, TEW-3, TEW-5 and  
 8 TEW-6) and TEW-5 is the only station showing such a vertical profile.

9

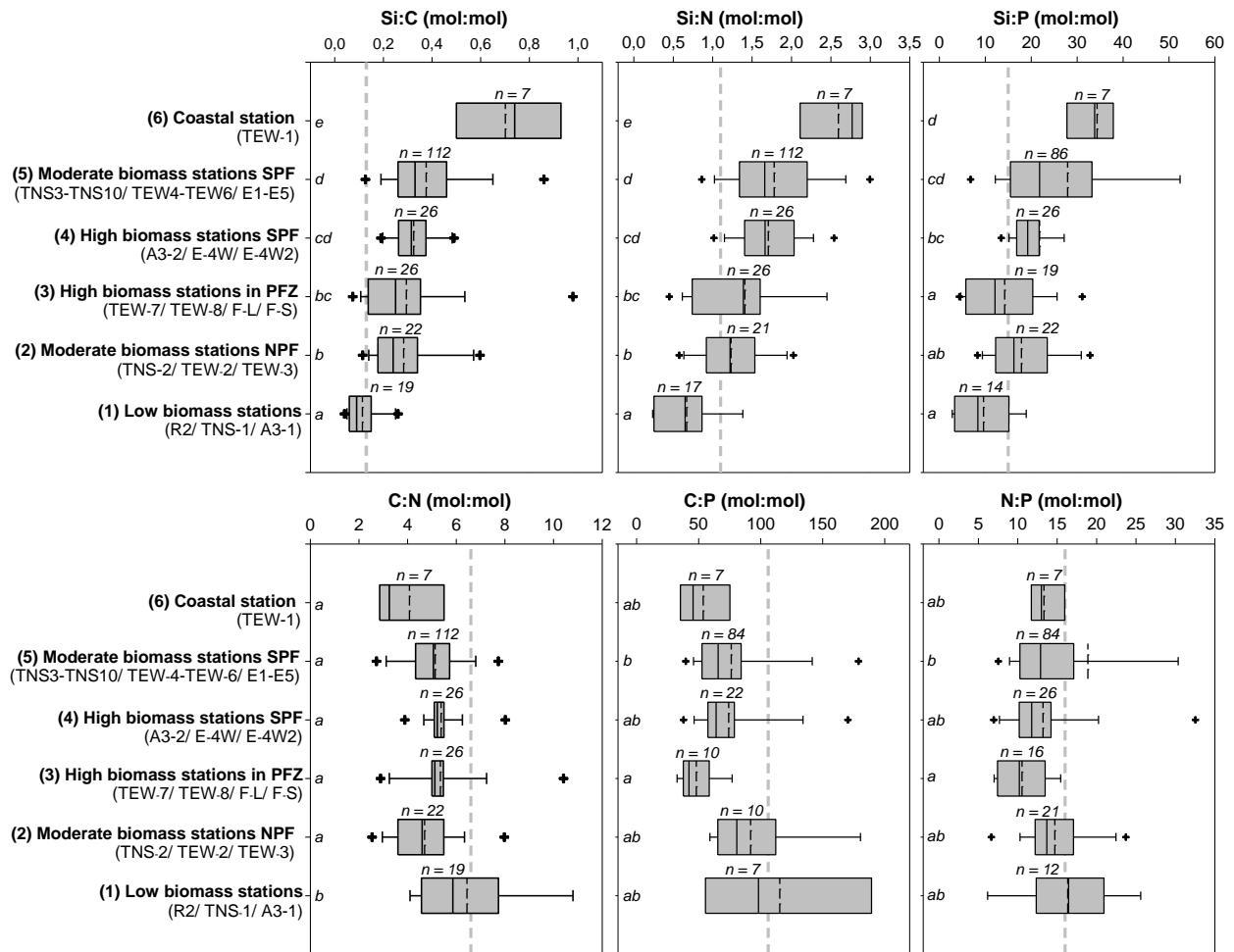


1

2 Figure 12. Temporal evolution of BSi concentrations within 200 m (a) (except for A3-2 where  
 3 data were integrated down to 160 m) and between 200 and 400 (b) for three size fractions  
 4 ( $> 0.8 \mu\text{m}$ , between  $0.8$  and  $20 \mu\text{m}$  and  $> 20 \mu\text{m}$ ) at the complex system of recirculation, at  
 5 the plateau reference station A3, at station E-4W (stations legend as in Fig. 7). The station F-  
 6 L and the HNLC reference station R2 are presented for comparison. At some stations, size-  
 7 fractionation was not performed because of logistical problems on-board.

8

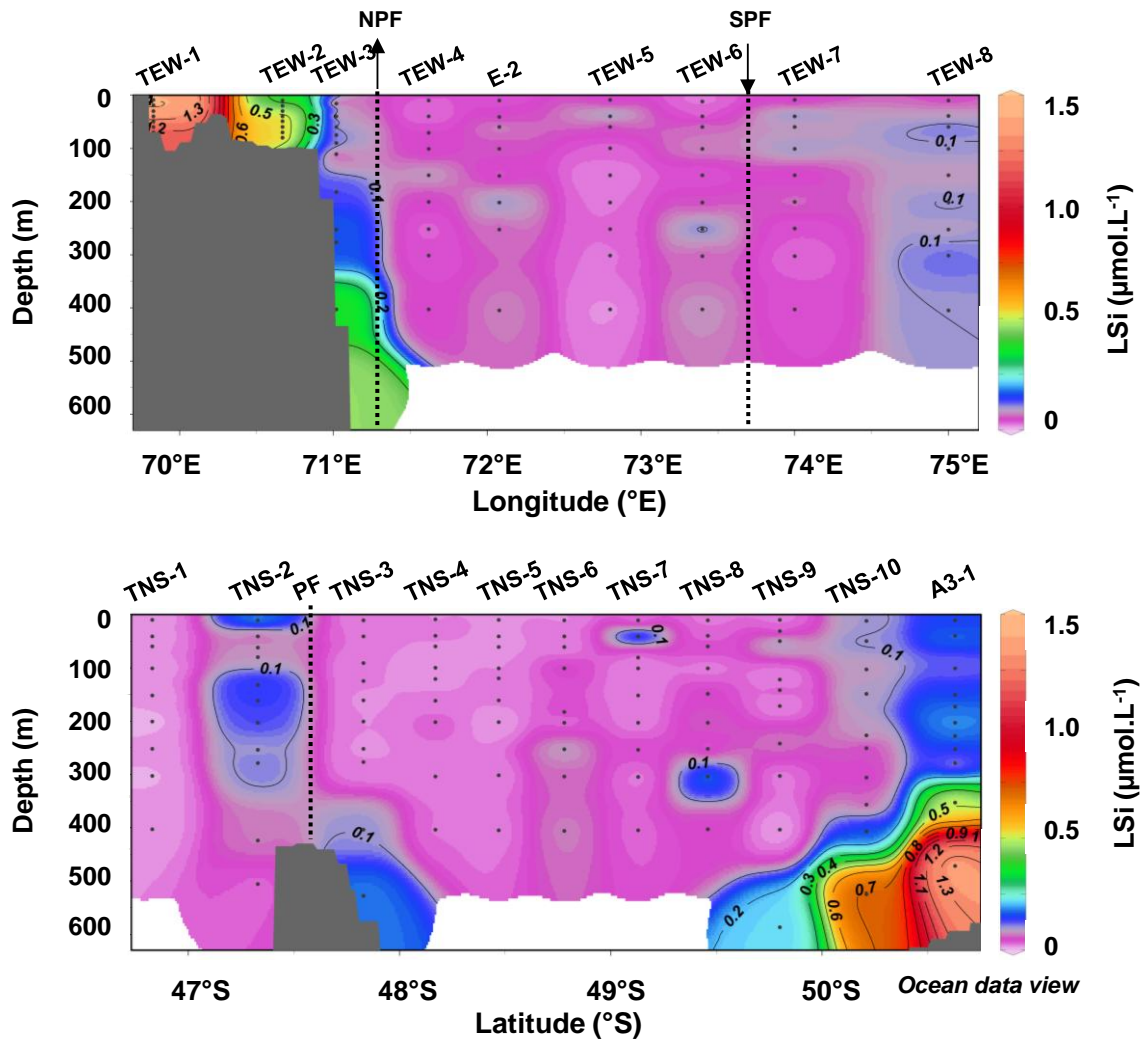
9



1

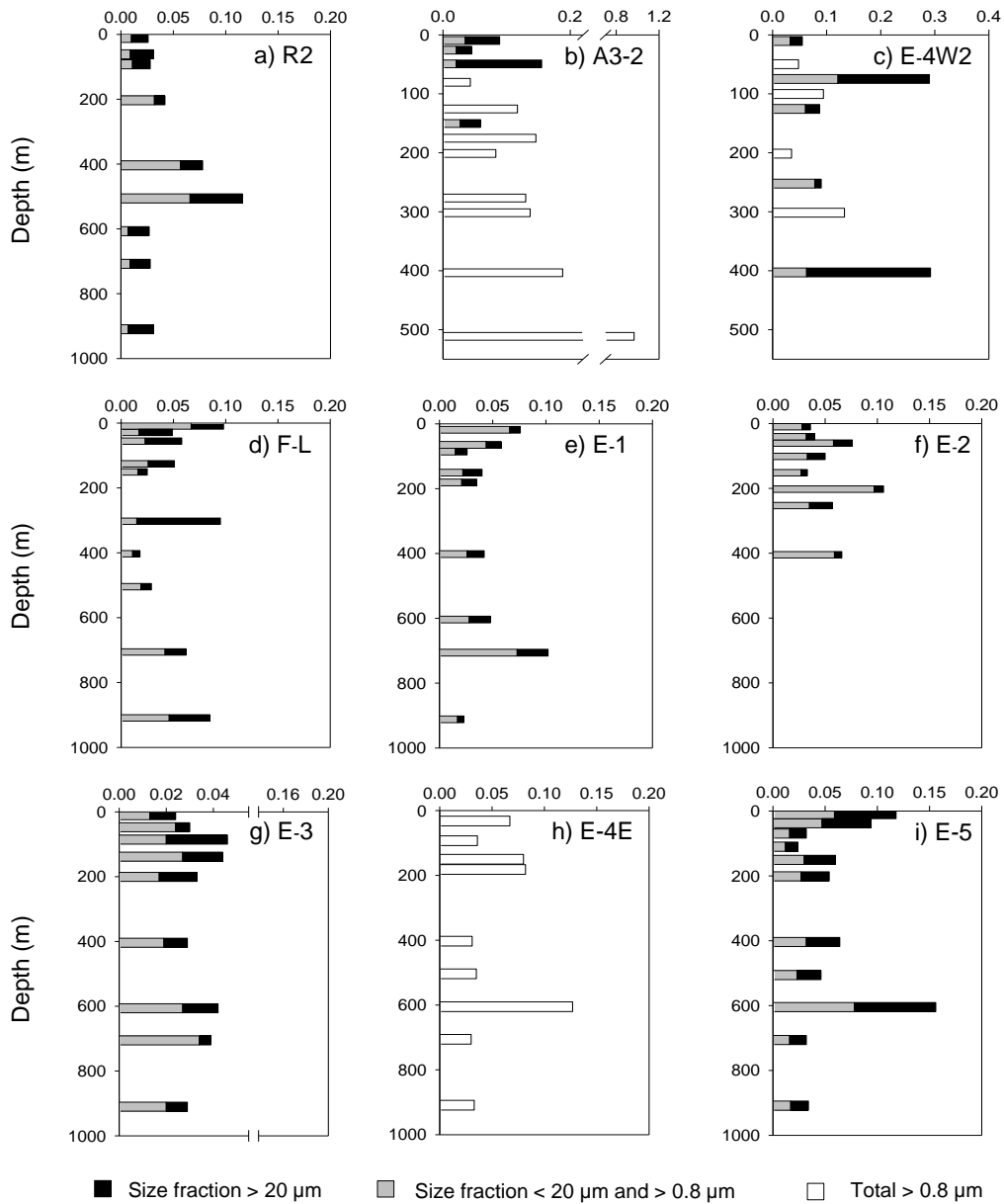
2 Figure 13. Box plots of the Si:C, Si:N, Si:P, C:N, C:P and N:P molar ratios within 200 m  
 3 (except for TEW-1 and TEW-2 where data were restricted within 70 m) for 6 clusters of  
 4 stations located in the Polar Front Zone (PFZ), north (NPF) and south of the Polar Front  
 5 (SPF). The length of the box corresponds to the distance between the 5<sup>th</sup> and the 95<sup>th</sup>  
 6 percentiles. The plain line and the dashed line inside the box represent the median and the  
 7 mean respectively. The vertical lines extend to the minimum and maximum values of the  
 8 cluster. The cross symbols correspond to outliers and “n” is the number of values in each  
 9 cluster. The grey dashed lines represent the typical values of Si:C (0.13), Si:N (1.1) and  
 10 Si:P (15) for nutrient-replete diatoms reported by Brzezinski (1985) and the typical values of  
 11 C:N (6.6), C:P (106) and N:P (16) reported by Redfield et al. (1963). The clusters of which  
 12 medians are not statistically different are indicated by the same letter (Mann-Whitney U-test,  
 13  $p > 0.05$ ).





1  
2  
3  
4  
5

Figure 14. Vertical distribution of lithogenic silica (LSi) concentrations along the TEW and TNS transects. The dotted lines represent the approximate location of the southern branch of the Polar Front going to the North (NPF) and to the South (SPF).



1

2 Figure 15. Vertical profiles of lithogenic silica (LSi) concentrations for three size fractions  
 3 (> 0.8  $\mu\text{m}$ , between 0.8 and 20  $\mu\text{m}$  and > 20  $\mu\text{m}$ ) at stations R2 (a), A3-2 (b), E-4W2 (c), F-L  
 4 (d) and at stations E: E-1 (e), E-2 (f), E-3 (g), E-4E (h), E-5 (i).